

## Accepted Manuscript

Molecular dynamics investigation of interfacial adhesion between oxidised bitumen and mineral surfaces

Yangming Gao, Yuqing Zhang, Yang Yang, Junhui Zhang, Fan Gu



PII: S0169-4332(19)30463-5

DOI: <https://doi.org/10.1016/j.apsusc.2019.02.121>

Reference: APSUSC 41816

To appear in: *Applied Surface Science*

Received date: 4 July 2018

Revised date: 6 February 2019

Accepted date: 13 February 2019

Please cite this article as: Y. Gao, Y. Zhang, Y. Yang, et al., Molecular dynamics investigation of interfacial adhesion between oxidised bitumen and mineral surfaces, *Applied Surface Science*, <https://doi.org/10.1016/j.apsusc.2019.02.121>

This is a PDF file of an unedited manuscript that has been accepted for publication. As a service to our customers we are providing this early version of the manuscript. The manuscript will undergo copyediting, typesetting, and review of the resulting proof before it is published in its final form. Please note that during the production process errors may be discovered which could affect the content, and all legal disclaimers that apply to the journal pertain.

## Molecular dynamics investigation of interfacial adhesion between oxidised bitumen and mineral surfaces

Yangming Gao<sup>1</sup>, Yuqing Zhang<sup>1\*</sup>, Yang Yang<sup>2</sup>, Junhui Zhang<sup>3</sup>, Fan Gu<sup>1</sup>

<sup>1</sup> Aston Institute of Materials Research, and Engineering Systems & Management Group  
Aston University, Birmingham, B4 7ET, U.K.

<sup>2</sup> Bioenergy Research Group, European Bioenergy Research Institute, Aston University, Birmingham,  
B4 7ET, U.K.

<sup>3</sup> National Engineering Laboratory of Highway Maintenance Technology, Changsha University of  
Science & Technology, Changsha, China.

\*corresponding author: [y.zhang10@aston.ac.uk](mailto:y.zhang10@aston.ac.uk); +44 (0)121 204 3391

### ABSTRACT

The interfacial adhesion between oxidised bitumen and mineral surfaces at dry and wet conditions was investigated using molecular dynamics (MD) simulations. Molecular models were built for virgin and oxidised bitumen components including saturate, aromatic, resin and asphaltenes. The bitumen models and four representative mineral substrates (namely quartz, calcite, albite and microcline) were employed to construct bitumen-mineral interface systems. These models were validated by the experimental results and MD simulations reported in the literature. The hardening mechanism of the aged bitumen was analysed by comparing the density, cohesive energy density and fraction of free volume between the virgin and oxidised bitumen. Work of adhesion was computed to quantify the adhesive bonding property of the bitumen-mineral interface systems for the virgin, lightly oxidised and heavily oxidised bitumen models under dry and wet conditions. Results show that the oxidised products (carbonyl and sulfoxide) strengthen the intermolecular bonding, resulting in molecular

aggregation and physical hardening of the aged bitumen. When bitumen becomes oxidised at the dry condition, the interfacial adhesion of bitumen-acidic minerals (quartz) is dominated by van der Waals interaction which decreases due to the increased bitumen-quartz intermolecular distance caused by the aggregated bitumen molecules during aging. In comparison, the interfacial adhesion of bitumen-strong alkali minerals (albite and microcline) is dominated by electrostatic energy which increases due to higher polarity introduced by the oxidised products. For the bitumen-weak alkali mineral (calcite), the interfacial adhesion is attributed to both electrostatic energy and van der Waals energy, where compared to the virgin bitumen, the electrostatic energy becomes lower for the lightly-oxidised bitumen due to the increased bitumen-mineral distance but becomes higher for the heavily-oxidised bitumen due to higher polarity. At wet condition, water is the dominating factor that affects (weakens) the interfacial adhesion between the bitumen and the acidic minerals (quartz), and the oxidative aging of bitumen is the major factor that affects (strengthens) the interfacial adhesion between the bitumen and the strongly alkaline minerals (albite and microcline). For the weak alkali minerals such as calcite, both water and bitumen aging can significantly affect the interfacial adhesion.

***Keywords***

Bitumen aging; interfacial adhesion; oxidised bitumen; mineral surfaces, molecular dynamics; water damage

## 1. Introduction

Bitumen is an important organic material for industrial applications, which is the refinery residues from petroleum (crude oil). As an adhesive and thermoplastic material, bitumen has been widely used for road pavement construction [1] and water-proofing coatings. In addition, it can also be used as an electrically conductive material when mixed with graphite particles [2]. Bitumen's durability is significantly affected by oxidative aging where bitumen molecules react with atmospheric oxygen [3]. The oxidative aging can cause chemical changes of the bitumen including the formation of carbonyl and sulfoxide, which have a considerable impact on the physical and mechanical properties of the bituminous materials, such as viscoelastic properties, cohesive and adhesive bond strengths, and fracture properties [4,5].

A number of experimental studies have been performed to understand the bitumen aging at the micro and macro dimensions in the pavement engineering applications. Rheological tests were developed to characterize and quantify the aging behaviour of the bitumen [6-9]. Recently, the aging effects of bitumen on the rheology [10,11], intrinsic healing [12], and surface energy and bonding property [13] were also evaluated using a variety of material characterisation technologies including Dynamic Shear Rheometer (DSR), Fourier Transform Infrared Spectroscopy (FTIR) and Atomic Force Microscopy (AFM) tests. It has been recognised that the oxidation causes the hardening of the bitumen, leading to a higher cracking susceptibility of the asphalt pavements [14]. While these experimental studies were commendable, they have not fully addressed the oxidative aging effects on the thermodynamic properties (such as intermolecular energies, interactions and cohesion) of bitumen at the atomistic and molecular scales. Aged bitumen with the introduction of oxygen atoms differs from virgin bitumen in terms of chemical composition that links closely to thermophysical behaviours of bitumen [15,16].

Molecular dynamics (MD) simulation is advantageous over the traditional laboratory-based methods in understanding the nanostructure and properties of the bitumen at the molecular scale [17]. Several studies using MD simulation have been carried out to investigate the physical property changes of the bitumen from the perspectives of chemical compositional or molecular structural changes due to the oxidative aging. Tarefder and Arisa [18] determined the changes in thermodynamic properties of asphaltene and resin in bitumen before and after oxidative aging based on the defined molecule structures [19,20]. Pan et al. [21] used the 3-component model bitumen system [22] to explore the molecular-scale processes of bitumen oxidation in the quantum chemistry (QC)-based environment and analysed the hardening mechanisms of bitumen's oxidation. Recently, Li and Greenfield [23,24] developed three 12-component model bitumen systems to represent the AAA-1, AAK-1 and AAM-1 bitumens used by the Strategic Highway Research Program (SHRP) and analysed the properties of the model bitumens using molecular simulation such as viscosity, relaxation time and dynamics. Pan and Tarefder [25] investigated the density, bulk modulus, viscosity and mechanical property changes of the 12-component AAA-1 model bitumen system before and after oxidative aging at room temperature (298 K). Xu and Wang [26] used the 12-component AAA-1 model bitumen system to analyse the intermolecular interactions of virgin and aged bitumen and to study the aging effects on self-healing and moisture damage of bitumen due to oxidation.

However, limited work has been focused on the effects of bitumen's oxidative aging on the adhesion of the bitumen-mineral interface at the molecular scale, particularly when the minerals are different and water are present. The authors' previous studies have found that the interfacial adhesion between the bitumen and aggregate played a critical role in determining the viscoelastic characteristics and cracking performance of the asphalt mixtures [27-31]. The interfacial interaction between bitumen and mineral surfaces has been investigated using

atomic force microscopy (AFM) and X-ray photoelectron spectroscopy (XPS) to improve the interfacial adhesion performance of asphalt mixture [32,33]. MD simulations have been used to quantify the adhesion properties and debonding behaviours between a virgin (unaged) bitumen and four different minerals [34]. It was found that the bitumen-mineral interfacial adhesion is primarily attributed to van der Waals force for neutral minerals (quartz) and to electrostatic interaction for alkali minerals (calcite, albite and microcline). This interfacial adhesion strength was greater for the alkali minerals than that of the neutral minerals. The adhesion would be significantly reduced when water presents. The authors' previous study used the virgin bitumen, thus it is unknown how the oxidative aging of the bitumen will alter the aforementioned findings. Therefore, there is a need for understanding the changes of the bitumen-mineral adhesion at the molecular scale when the bitumen becomes oxidatively aged to different levels, which is investigated in the study.

The main objective of this study is to investigate the interfacial adhesion between oxidised bitumen and mineral surfaces using molecular dynamics (MD) simulation method. Molecular models of virgin and oxidised bitumen were constructed based on saturate, aromatic, resin and asphaltene (SARA) four fractions. The bitumen models together with four different mineral substrates (quartz, calcite, albite and microcline) were employed to build bitumen-mineral interface systems. The molecular models were validated by the laboratory results from the experiments or simulations reported in the literature. The hardening mechanism of aged bitumen was analysed using the molecular models of the virgin and oxidised bitumen. The adhesive bond energy of the bitumen-mineral interface systems was quantified by the work of adhesion and the effects of oxidative aging on the bitumen-mineral adhesion were investigated at dry and wet conditions.

## 2. Modelling of virgin and oxidised bitumen components

Bitumen is a chemical mixture composed of a wide variety of hydrocarbons with the heteroatoms such as oxygen, sulphur and nitrogen atoms, which leads to the chemical complexity of the bitumen. Modern separation techniques divide bitumen into different fractions according to their similarity in terms of polar and molecular characteristics. Based on the concept of four fractions proposed by American Society for Testing and Materials (ASTM) D4124-09, a bitumen can be separated into saturates, aromatics, resins and asphaltenes (SARA) four components.

Asphaltenes act as the viscosity-building agents in bitumen and are the largest and most polar component fraction in the bitumen system. They consist of the condensed aromatic and naphthenic molecules with a trace amount of heteroatoms (O, S and N) [35]. Three different types of asphaltenes (asphaltene-phenol, asphaltene-pyrrole and asphaltene-thiophene) are used to represent asphaltene fraction in the bitumen system. These asphaltene molecular structures modelled the laboratory measurements and calculations, thus being capable of representing the true asphaltenes [36,37]. The molecular structures of the virgin asphaltene fraction are shown in **Fig. 1(a)**. Resins (polar aromatics) are the second polar fraction in bitumen and act as the stabilizer for the asphaltenes [38]. Heteroatoms such as oxygen, sulphur and nitrogen are also found in resin molecules composed of polar aromatic rings and long non-polar paraffinic groups. **Fig. 2(a)** shows the five different molecules (quinolinohopane, thioisorenieratane, benzobisbenzothiophene, pyridinohopane and trimethylbenzene-oxane) used to represent the virgin resin fraction. These molecular models were selected based on the analyses of petroleum found in sedimentary rock deposits in the geochemistry studies [39-43]. Aromatics (naphthene aromatics) are the softening component in bitumen and have the minimal polarity in the bitumen system. They are hydrocarbons structures with light molecular weights. **Fig. 3(a)** illustrates the molecular models of the

virgin aromatic fraction, which are named as perhydrophenanthrene-naphthalene (PHPN) and dioctyl-cyclohexane-naphthalene (DOCHN), respectively. PHPN was proposed as a main aromatic compound [44] and DOCHN was shown as another common naphthene aromatic structure on the basis of the n-d-M method [45]. Saturates consist of the normal, branched and cyclic alkanes, which rarely change with time due to the lack of polar chemical functional groups. Squalane and hopane shown in **Fig. 4** are selected as representative saturate fraction, which is consistent with the findings from the direct separation and quantitative determination of n- and iso-alkanes in neat SHRP (Strategic Highway Research Program) bitumen using urea adduction and high temperature gas chromatography (HTGC) by Netzel and Rovani [46]. The specific selections of these molecular models for asphaltenes, resins, aromatics and saturates were reported and explained in detail by previous experimental and simulation studies [23].

Bitumen composition changes when it is exposed to atmospheric oxygen. New chemical functional groups are formed in bitumen, which is responsible for the increase of the viscosity [3]. Extensive experimental studies have been conducted to investigate the mechanism of bitumen aging due to oxidation. It was found that there are two types of the readily oxidizable locations in bitumen. One is the carbon atom adjacent to an aromatic ring. The hydrogen atom attached to the benzylic carbon atom is displaced by oxygen to form a ketone. The other is sulphide that reacts with oxygen to form sulfoxide. The sulfoxides formed at sulphur atoms and ketones formed at benzylic carbon atoms have been identified as the major oxidation products [15, 47].

Asphaltene and resin contain the chemically functional groups of oxygen, sulphur and nitrogen atoms, which results in their high polarity. Therefore, they have strong interaction and are highly reactive with the electronegative oxygen. King and Corbett showed that aromatic was slightly oxidized and saturate were relatively inert to the reaction with oxygen

due to the lack of sensitive functional groups [48]. Based on the oxidation mechanism discussed above, the ketones and sulfoxides were added to the possible oxidizable sites of the 12-component bitumen model to build the oxidised bitumen molecular models due to aging. **Figs. 1(b)-3(b)** show the molecular structures of the oxidised asphaltene, resin and aromatic fractions in the aged bitumen, respectively [25]. The saturate fraction has been assumed to remain unchanged during the oxidative aging. It is noted that the saturate volatilization is also one of the mechanisms causing aging in bitumen in addition to oxidation. The study of volatilization was not considered in this study due to the following reasons: (a) Volatilization mainly occurs during the mixing and compaction of asphalt mixtures at high temperatures such as 150 °C or even higher. This contributes to the short-term aging rather than the long-term aging. The research scope of this study was focused on the long-term aging mechanism involving the formation of ketone and sulfoxide functional groups due to oxidation in bitumen. (b) Volatilization is a time-dependent process. It is still a numerical challenge to study a time-dependent process such as volatilization taking more than seconds in classical MD simulations. Thus the authors decided to focus the study on the long-term aging of bitumen due to oxidation, which is also the primary contributor for the bitumen's aging. The short-term aging mechanisms including volatilization will be investigated by the laboratory study in the future.

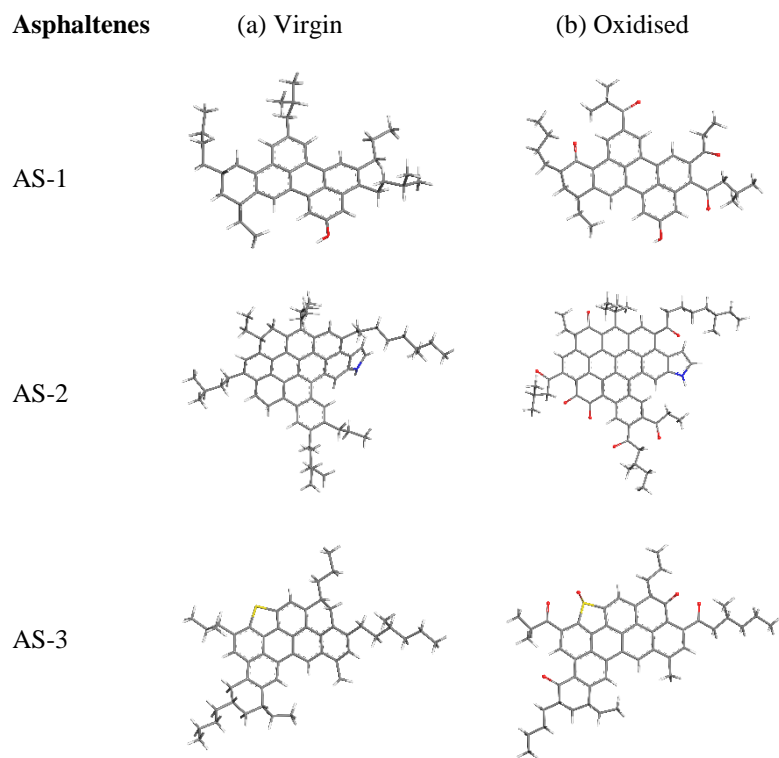


**Fig. 1.** Molecular structures of asphaltene fraction (AS-1, asphaltene-phenol; AS-2, asphaltene-pyrrole; AS-3, asphaltene-thiophene). (a) Virgin asphaltene molecules [23]. (b) Oxidised asphaltene molecules [25]. (Carbon atoms are grey, hydrogen atoms are white, oxygen atoms are red, sulphur atoms are yellow, and blue is nitrogen).

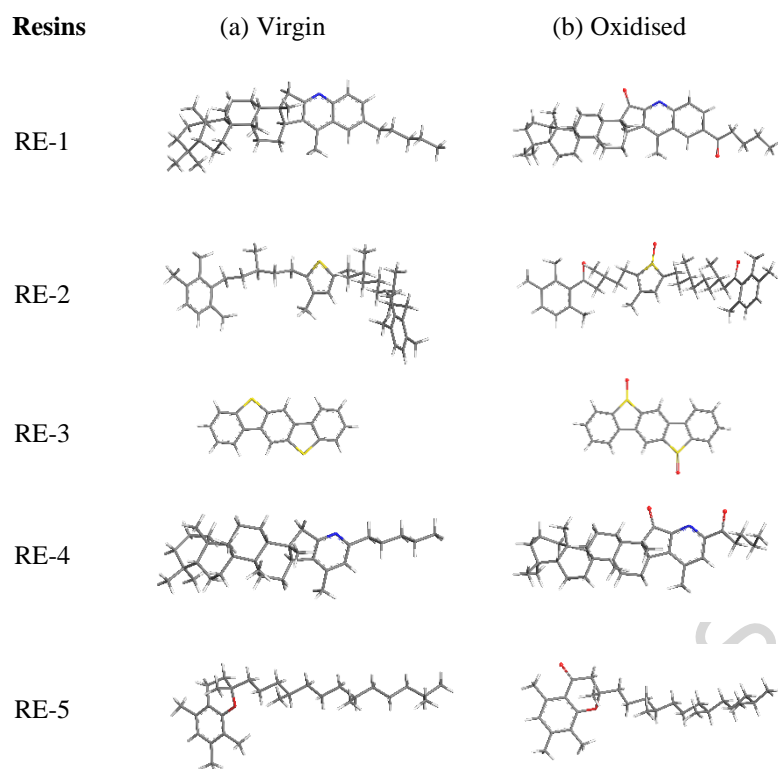


**Fig. 2.** Molecular structures of resin fraction (RE-1, quinolinohopane; RE-2, thioisorenieratane; RE-3, benzobisbenzothiophene; RE-4, pyridinohopane; RE-5, trimethylbenzene-oxane). (a) Virgin resin molecules [23]. (b) Oxidised resin molecules [25].

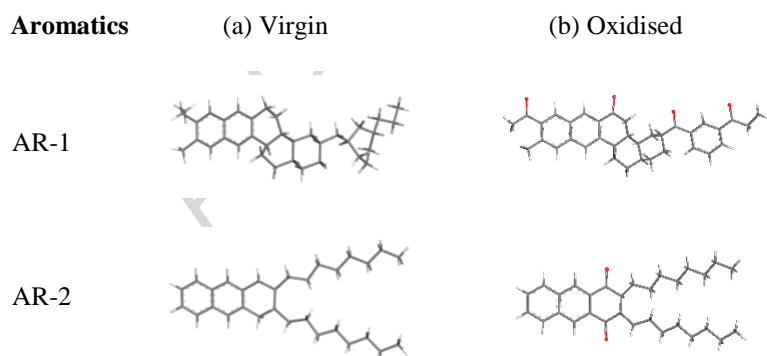


**Fig. 3.** Molecular structures of aromatic fraction (AR-1, PHPN; AR-2, DOCHN). (a) Virgin aromatic molecules [23]. (b) Oxidised aromatic molecules [25].

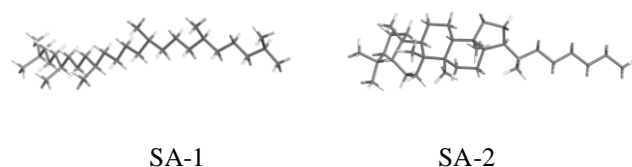


**Fig. 4.** Molecular structures of saturate fraction (SA-1, squalane; SA-2, hopane) [23].

### 3. Molecular dynamics (MD) simulation method

#### 3.1 Virgin and oxidised model bitumen systems

Based on the molecular models of the virgin and oxidised bitumen components presented in **Section 2**, the virgin and aged model bitumen systems were constructed in this section. The SHRP AAA-1 model bitumen system developed by Li and Greenfield [23] is chosen for this study, which has been demonstrated to have the similar or equivalent chemical and mechanical properties and performance to a real bitumen. The number of each type of the component molecules in the virgin and aged model bitumen systems can be seen in **Table 1**.

To build the virgin model bitumen system, all these molecules of the virgin bitumen were put into a cubic simulation box to form a bulk bitumen model. The initial density of the box was set as  $0.1 \text{ g/cm}^3$  to ensure the random distribution of the molecules. A geometry optimization process for 5000 iterations was first conducted to minimize the system energy. The system was then subjected to molecular dynamic (MD) equilibration under the NPT ensemble (in which the number of particles, pressure, and temperature were controlled unchanged) for 100 ps with 1.0 fs time step to obtain a stable system volume. The MD simulation was performed at a temperature of 298 K and a pressure of 1.0 atm. After which, NVT ensemble (where the number of particles, system volume, and temperature were controlled unchanged) at 298 K

was used to further equilibrate the system for 100 ps to generate an equilibrated model bitumen system with stable volume and energy fluctuation.

For the aged model bitumen systems, two oxidation levels, namely lightly-oxidised bitumen (LOB) and heavily-oxidised bitumen (HOB), are considered in this study by assigning a different number of the oxidised molecules in a model bitumen system, as shown in **Table 1**. The number of the oxidised molecules in the lightly-oxidised bitumen is half of that in the heavily-oxidised bitumen. This method has been employed to model the aging of bitumen at different oxidation levels in the previous studies [17,25]. The aged model bitumen systems were built following the same procedure as the virgin model bitumen system above. **Fig. 5** shows the final structures of the model bitumen systems at different oxidation levels.

**Table 1** Molecular compositions of the SHRP AAA-1 model bitumen system at different oxidation levels used for MD simulations.

Label	Molecules in model		Molecular formula	Number of molecules		
				VB <sup>a</sup>	LOB <sup>b</sup>	HOB <sup>c</sup>
SA-1	Saturate	Squalane	C <sub>30</sub> H <sub>62</sub>	4	4	4
SA-2		Hopane	C <sub>29</sub> H <sub>50</sub>	4	4	4
AR-1	Aromatic	PHPN	C <sub>35</sub> H <sub>44</sub>	11	6	0
OAR-1		Oxidised PHPN	C <sub>35</sub> H <sub>36</sub> O <sub>4</sub>	0	5	11
AR-2	aromatic)	DOCHN	C <sub>30</sub> H <sub>46</sub>	13	7	0
OAR-2		Oxidised DOCHN	C <sub>30</sub> H <sub>42</sub> O <sub>2</sub>	0	6	13
RE-1	Resin	Quinolinhopane	C <sub>40</sub> H <sub>59</sub> N	4	2	0
ORE-1		Oxidised Quinolinhopane	C <sub>40</sub> H <sub>55</sub> NO <sub>2</sub>	0	2	4
RE-2	aromatic)	Thioisorenieratane	C <sub>40</sub> H <sub>60</sub> S	4	2	0
ORE-2		Oxidised Thioisorenieratane	C <sub>40</sub> H <sub>56</sub> SO <sub>3</sub>	0	2	4
RE-3		Benzobisbenzothiophene	C <sub>18</sub> H <sub>10</sub> S <sub>2</sub>	15	8	0
ORE-3		Oxidised Benzobisbenzothiophene	C <sub>18</sub> H <sub>10</sub> S <sub>2</sub> O <sub>2</sub>	0	7	15
RE-4		Pyridinohopane	C <sub>36</sub> H <sub>57</sub> N	4	2	0

ORE-4		Oxidised Pyridinohopane	$C_{36}H_{53}NO_2$	0	2	4
RE-5		Trimethylbenzene-oxane	$C_{29}H_{50}O$	5	3	0
ORE-5		Oxidised Trimethylbenzene-oxane	$C_{29}H_{48}O_2$	0	2	5
AS-1	Asphaltene	Asphaltene-phenol	$C_{42}H_{50}O$	3	2	0
OAS-1		Oxidised Asphaltene-phenol	$C_{42}H_{46}O_5$	0	1	3
AS-2		Asphaltene-pyrrole	$C_{66}H_{81}N$	2	1	0
OAS-2		Oxidised Asphaltene-pyrrole	$C_{66}H_{67}NO_7$	0	1	2
AS-3		Asphaltene-thiophene	$C_{51}H_{62}S$	3	2	0
OAS-3		Oxidised Asphaltene-thiophene	$C_{51}H_{54}SO_5$	0	1	3

<sup>a</sup> VB, virgin bitumen. The number of each molecule in VB is based on the Li and Greenfield's work [23];

<sup>b</sup> LOB, the lightly-oxidised bitumen;

<sup>c</sup> HOB, the heavily-oxidised bitumen.

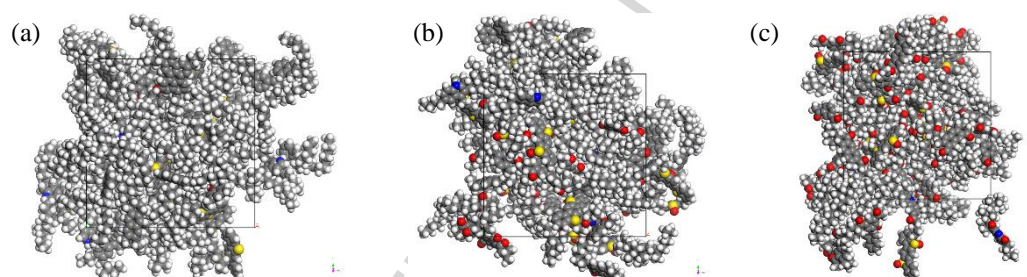


**Fig. 5.** Model bitumen systems built for MD simulations. (a) Virgin model bitumen system. (b) Lightly-oxidised model bitumen system. (c) Heavily-oxidised model bitumen system.

### 3.2 Construction of the bitumen-mineral interface systems

In order to construct the bitumen-mineral interface system models, the mineral substrate and bitumen layer models are first prepared following the method described in the authors' previous work [34].

Quartz, calcite, albite and microcline are selected to build the mineral substrate models. The four types of minerals commonly exist in the aggregates such as granite, limestone and basalt used for constructing asphalt concrete. To model the mineral substrate, the crystal unit cell

was firstly cleaved along the Miller plane (100) to expose the corresponding surface and then this surface was extended to create an orthogonal mineral supercell with the periodic boundary condition in all three dimensions. The basis for selecting Miller plane (100) is built upon an evaluation the effects of different Miller planes on the interfacial adhesion simulation results. Three Miller planes (100), (010) and (001) of a mineral (using quartz as an example) were used and the results obtained from the three Miller planes showed a minor difference, indicating that the use of Miller plane would have little effect on the qualitative analysis of the interfacial adhesion. Since the Miller plane (100) makes the interface model with the minimum lattice mismatch for the four minerals, the Miller plane (100) was therefore selected in the study. The details of four mineral substrates are shown in **Table 2**.

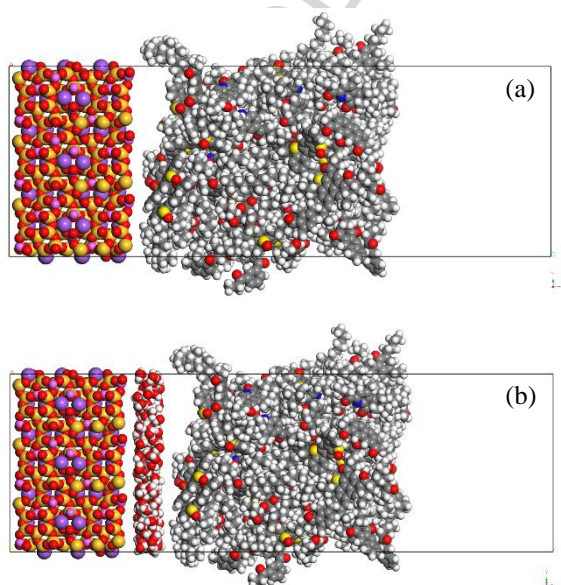
The bitumen layer was built with the same width and length as the mineral substrate. The layer model was subjected to a geometry optimization followed by an MD simulation of 100 ps with NVT ensemble to equilibrate the system.

**Table 2** Details of four mineral substrates used for MD simulations.

Minerals	Chemical formula	Lattice parameters of unit cell	Supercell size ( $\text{\AA} \times \text{\AA} \times \text{\AA}$ )
Quartz	$\text{SiO}_2$	$a=b=4.910 \text{ \AA}$ , $c=5.402 \text{ \AA}$ $\alpha=\beta=90^\circ$ , $\gamma=120^\circ$	$39.28 \times 37.81 \times 20.36$
Calcite	$\text{CaCO}_3$	$a=b=4.990 \text{ \AA}$ , $c=17.061 \text{ \AA}$ $\alpha=\beta=90^\circ$ , $\gamma=120^\circ$	$34.93 \times 34.12 \times 23.65$
Albite	$\text{NaAlSi}_3\text{O}_8$	$a=8.115 \text{ \AA}$ , $b=12.762 \text{ \AA}$ , $c=7.158 \text{ \AA}$ $\alpha=94.218^\circ$ , $\beta=116.803^\circ$ , $\gamma=87.707^\circ$	$38.29 \times 35.79 \times 22.10$
Microcline	$\text{KAlSi}_3\text{O}_8$	$a=8.573 \text{ \AA}$ , $b=12.962 \text{ \AA}$ , $c=7.219 \text{ \AA}$ $\alpha=90.567^\circ$ , $\beta=115.917^\circ$ , $\gamma=87.750^\circ$	$38.89 \times 36.10 \times 23.89$

Once the developed bitumen layer and mineral substrate models were obtained, the bitumen-mineral interface system models could be constructed. The bitumen layer was firstly combined with the mineral substrate and then a vacuum layer of  $30 \text{ \AA}$  was placed over the top

surface of the bitumen layer in order to avoid interaction across the mirror image in the z-direction. For the wet interface model, a layer containing 200 water molecules was added at the bitumen-mineral interface to form a bitumen-water-mineral interface system. The dry and wet interface systems for the heavily-oxidised bitumen with albite substrate are illustrated in **Figs. 6(a)** and **(b)**. After a geometry optimization process, the interface systems were subjected to dynamics equilibration with NVT ensemble for 100 ps to reach the stable state. The simulation time was selected as 500 ps for the bitumen-mineral interface system, which is demonstrated to be sufficiently long to reach an equilibration. As shown in **Fig. 6(c)**, a stable energy system (including potential energy and non-bond energy) has been reached after the first 100 ps. In this study, an additional 400 ps simulation under the NVT ensemble was performed on all bitumen-mineral interface systems for the subsequent trajectory analysis and calculations. To support our assertion, a MD study with a longer simulation time (1.2 ns) was performed, in which the bitumen/albite interface model was used as an example. It was also found that the work of adhesion ( $1328.73 \text{ mJ/m}^2$ ) obtained from 1.2 ns simulation coincides with the result ( $1257.25 \text{ mJ/m}^2$ ) using 500 ps as the simulation time. Therefore, the simulation time (500 ps) used is reasonable considering the balance between the accuracy of simulation results and the computational time consumed.



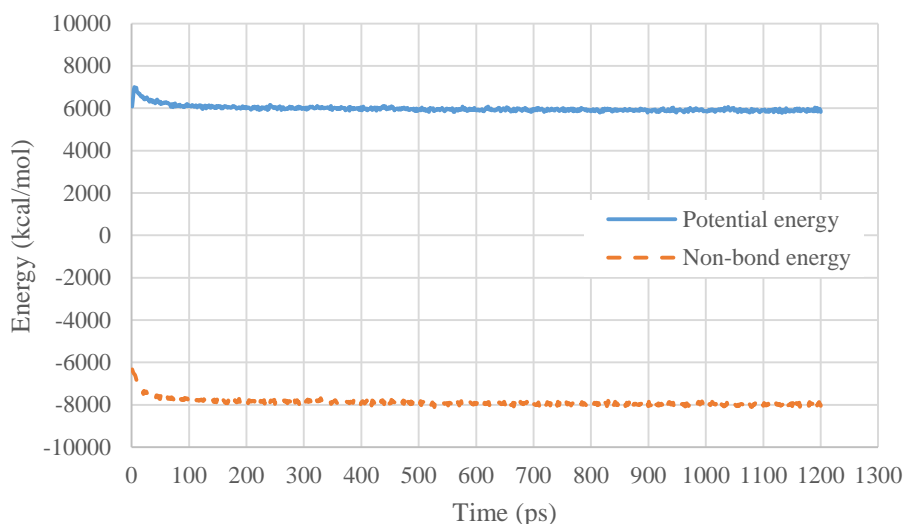


**Fig. 6.** Interface systems between a heavily-oxidised bitumen and an albite substrate. (a) The heavily-oxidised bitumen-albite model. (b) The heavily-oxidised bitumen-water-albite model. (c) The convergence of energies during the simulation for the virgin bitumen-albite model.

### 3.3 Force field and simulation parameters

In MD simulations, the interatomic interactions are characterised by force field that defines the interatomic potential. The Condensed-phase Optimized Molecular Potentials for Atomistic Simulation Studies (COMPASS) force field is adopted in this study, which is an *ab initio* force field and is able to predict dynamics of organics, inorganics and their interface systems. The COMPASS force field has a broad coverage in covalent molecules including most common organics (polymers), more importantly, it has an extended coverage for the inorganic materials (metals, metal oxides, and metal halides using various non-covalent models). The combination of force field parameters for organics and inorganics makes the COMPASS force field possible to study the interfacial interaction in the mixed systems. The COMPASS force field parameters have been validated using various calculation methods [49] and it has been successfully applied for the study of the bitumen-mineral interfacial systems [34, 50, 51].

The potential energy ( $E$ ) in the COMPASS force field is comprised of valence (or bonded) interactions ( $E_{\text{val}}$ ) and non-bonded interactions ( $E_{\text{nb}}$ ), as expressed in **Eq. (1)** [49].

$$E = E_{\text{val}} + E_{\text{nb}} \quad (1)$$

The valence interactions ( $E_{\text{val}}$ ) are contributed by covalent bonds between atoms, while the non-bonded interactions ( $E_{\text{nb}}$ ) include Coulomb electrostatic ( $E_{\text{Q}}$ ) and van der Waals ( $E_{\text{vdW}}$ ) terms, as shown in **Eq. (2)** [52].

$$E_{\text{nb}} = E_{\text{Q}} + E_{\text{vdW}} \quad (2)$$

The electrostatic interactions describe the Coulombic forces between two charged atoms. The electrostatic energy ( $E_{\text{Q}}$ ) is calculated using the Coulombic function

$$E_{\text{Q}} = \sum_{ij} \frac{q_i q_j}{r_{ij}} \quad (3)$$

where  $r_{ij}$  is the distance between atoms  $i$  and  $j$ , and  $q_i$  and  $q_j$  are the atomic charges, respectively.

The van der Waals interactions describe the van der Waals forces between two atoms, which are the sum of the intra and inter molecular attractive or repulsive interactions. The van der Waals energy ( $E_{\text{vdW}}$ ) is calculated using the Lennard-Jones (LJ) 9-6 potential

$$E_{\text{vdW}} = \sum_{ij} \varepsilon_{ij} \left[ 2 \left( \frac{r_{ij}^0}{r_{ij}} \right)^9 - 3 \left( \frac{r_{ij}^0}{r_{ij}} \right)^6 \right] \quad (4)$$

where  $r_{ij}$  is the distance between atoms  $i$  and  $j$ ,  $r_{ij}^0$  and  $\varepsilon_{ij}$  denote the LJ-9-6 parameters (constant) for the  $ij$  atom pair, respectively.

In this study, all these simulations were performed at 298 K with a time step of 1 fs. Ewald summation method was applied for the electrostatic interactions, and atom-based summation with a cut-off distance of 15.5 Å was used for the van der Waals interactions. Nose-Hoover-Langevin (NHL) thermostat and Andersen barostat were applied to control the temperature and pressure, respectively. These simulation parameters were extensively tested and

successfully applied for MD simulation studies of bituminous materials [26,34].

#### 4. Characterisation of the bitumen-mineral interfacial adhesion

To quantify the adhesion between bitumen and mineral, the adhesive bond energy of the bitumen-mineral interface systems is characterised by the work of adhesion. It is defined as the energy required to separate a unit area of the bitumen-mineral interface into a bitumen surface and a mineral surface. The work of adhesion ( $W_{BM}$ ) is expressed as [50,34]

$$W_{BM} = \Delta E_{BM} / A \quad (5)$$

$$\Delta E_{BM} = E_B + E_M - E_{BM} \quad (6)$$

where  $\Delta E_{BM}$  is the interaction energy between bitumen and mineral in the bitumen-mineral system;  $E_B$ ,  $E_M$ , and  $E_{BM}$  represent the potential energies of the bitumen layer, mineral substrate, and bitumen-mineral system at a thermodynamic equilibrium, respectively; and  $A$  is the interface contact area between bitumen and mineral.

Note that these parameters in **Eqs. (5) and (6)** are calculated based on the bitumen-mineral models and the bitumen-water-mineral models at the equilibrium state in order to determine the work of adhesion between bitumen and mineral at dry and wet conditions, respectively.

### 5. Results and discussion

#### 5.1 Model validation and hardening mechanism of aged bitumen

To validate the molecular simulation method and analyse the hardening mechanisms of bitumen due to oxidative aging at the molecular level, the thermophysical properties of virgin and aged bitumen were calculated including density, cohesive energy density (CED), and fraction of free volume (FFV).

The density of the bulk bitumen model at different oxidation levels was calculated at the

temperature of 298 K (25°C) based on MD simulations. **Fig. 7** shows the bitumen density changes due to oxidative aging. The bitumen density became higher after oxidative aging, where the density was 1.016 g/cm<sup>3</sup> for the lightly-oxidised bitumen and 1.048 g/cm<sup>3</sup> for the heavily-oxidised bitumen and the density was 0.981 g/cm<sup>3</sup> for the virgin bitumen. This trend is in good agreement with Pan and Tarefder's results [25] as well as the experimental results for the virgin and aged PG 58-28 bitumen [53]. It can also be seen from **Fig. 7** that the density change for simulation results before and after oxidative aging was greater than that of the experimental results. This is because the loss of volatile components due to the volatilisation during the aging process was not considered in the simulation.

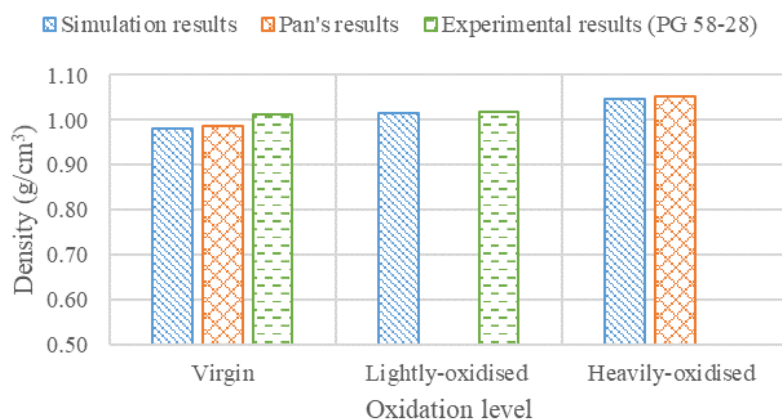


**Fig. 7.** Density of bulk bitumen model at different oxidation levels. (Note Pan's results [25] for lightly-oxidised bitumen and the experimental results [53] for heavily-oxidised bitumen are not available.)

Cohesive energy density (CED) is used to calculate the cohesive energy per unit volume to evaluate the intermolecular bonding strength of a bulk bitumen model. The cohesive energy is attributed to the non-bonded interactions including van der Waals and electrostatic interactions. **Fig. 8** shows the calculated CED for the bulk bitumen model at different oxidation levels including the van der Waals and electrostatic components. It was found that the CED value increased with the increasing oxidation level and the majority of the CED resulted from Van der Waals interaction. This indicates that the intermolecular bonding in

oxidised bitumen is stronger than that in the virgin bitumen. This is mainly due to that, when the oxygen atoms are introduced to bitumen, both the molecular weight and the polarity of the oxidised bitumen became higher than that of the virgin bitumen, which results in a greater van der Waals and electrostatic intermolecular interactions in the bulk bitumen model.

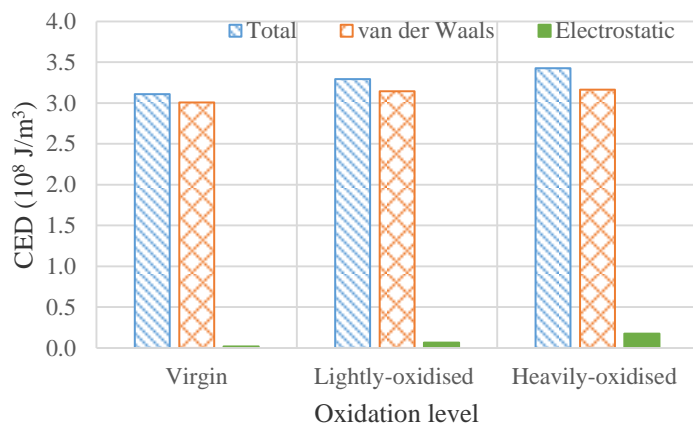


**Fig. 8.** Cohesive energy density (CED) of bulk bitumen model at different oxidation levels including two components, namely van der Waals and electrostatic intermolecular interactions.

The fraction of free volume (FFV) is used as a measure of the volume that has not been occupied by the molecules and to determine the percentage of volume available in a bulk bitumen model. **Fig. 9** shows the calculated FFV of the bulk bitumen model at different oxidation levels. The FFV value for the oxidised bitumen (approximately 37.5% for both the lightly-oxidised bitumen and the heavily-oxidised bitumen) was lower than that of virgin bitumen (38.2%). This means that the oxidised bitumen is agglomerate further than the virgin bitumen due to a higher molecular weight and polarity of the oxidised bitumen system.

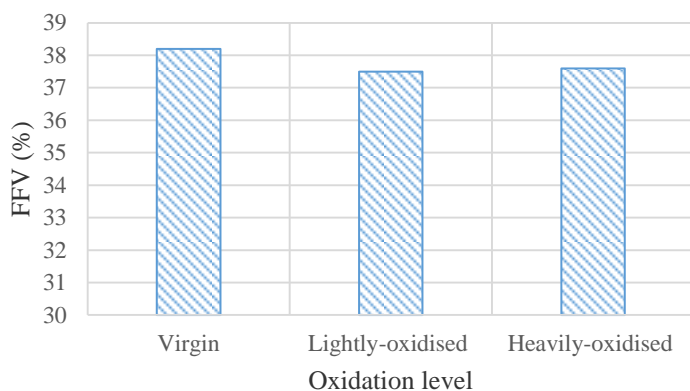


**Fig. 9.** Fraction of free volume (FFV) of the bulk bitumen model at different oxidation levels.

The lower FFV for the oxidised bitumen is consistent with the higher density and CED, which demonstrates a stronger intermolecular bonding in the oxidised bitumen system that leads to a further shrinkage of the bitumen system when oxygen is present in the material. The analysis of the thermophysical properties of the virgin and aged bitumen from the molecular perspective explains the physical hardening happened during the oxidative aging which was recognised through a number of experimental studies at the macroscopic level [14]. This also demonstrates the molecular simulation method is suitable for describing the aging behaviours of the bitumen due to oxidation and can be further applied for the investigation of the aged bitumen-mineral interface behaviours.

### 5.2 Molecular structure of bitumen on the mineral surfaces

Bitumen is regarded as a colloidal structure where asphaltene is dispersed in the maltene composed of resins, aromatics and saturates [38,54]. **Fig. 10** illustrates the nanostructures of bitumen at the heavily-oxidised bitumen-quartz interface and the heavily-oxidised bitumen-water-quartz interface obtained from the last frame of simulation trajectories, respectively. It can be observed that within the interfacial systems, asphaltene molecules (in blue colour) were dispersed in the maltene medium. Asphaltenes tended to form the nano-aggregation structures without a continuous network. This type of structure is also referred to bitumen sol-

gel structure, which has been reported in prior experimental and simulation studies [38,54].

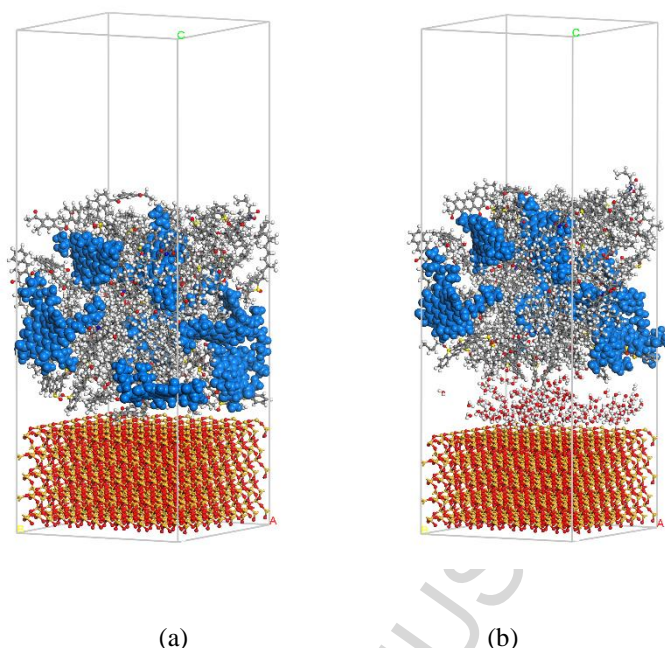


**Fig. 10.** Nanostructures of bitumen at (a) heavily-oxidised bitumen-quartz interface and (b) heavily-oxidised bitumen-water-quartz interface obtained from MD simulations. The asphaltene molecules (in blue colour) were dispersed in the maltene medium composed of resins, aromatics and saturates.

To characterise the molecular arrangement and mobility of bitumen on the mineral surfaces, the radial distribution function (RDF) and mean squared displacement (MSD) of the asphaltenes were analysed, respectively. RDF describes the probability of finding a particle at a radial distance  $r$  away from a reference particle in a system of particles. In this study, the intermolecular distance was calculated based on the asphaltene molecule's centre of mass. The trajectory obtained from the last 200 ps of MD simulations under NVT ensemble was applied for RDF analysis. **Fig. 11** shows the RDFs of asphaltene-asphaltene pair in the bitumen-microcline interfacial models at different oxidation levels. Radial distances corresponding to the first peak value of RDF curves for asphaltene-asphaltene pair in bulk bitumen model and four interfacial models at different oxidation levels were summarised in **Table 3**. In bulk bitumen models, the first peak value of RDF for the virgin bitumen occurred around 10-11 Å, while the distance became smaller for the heavily-oxidised bitumen (8-9 Å)

and the lightly-oxidised bitumen (4-5 Å). This indicates that the oxidative aging strengthened the bitumen's aggregation due to the higher molecular polarity, which is consistent with the finding in **Section 5.1**. In the interfacial models, it can be found from **Table 3** that the mineral surfaces had a significant influence on the nano-aggregation structure of the bitumen, especially under the oxidation conditions. The aggregation of the bitumen on the quartz surface was consistent with that of the bulk bitumen because of the very weak interaction between quartz and bitumen. The aggregation of the oxidised bitumen on the calcite surface was weakened since calcite attracted a part of the oxidised bitumen from the bulk bitumen due to the slightly strong electrostatic interaction. While for albite and microcline the very strong electrostatic interaction with bitumen has significantly strengthened the aggregation of the oxidised bitumen through attracting all the bitumen molecules to their surfaces, demonstrated by the reduced first peak position when the bitumen became oxidised.

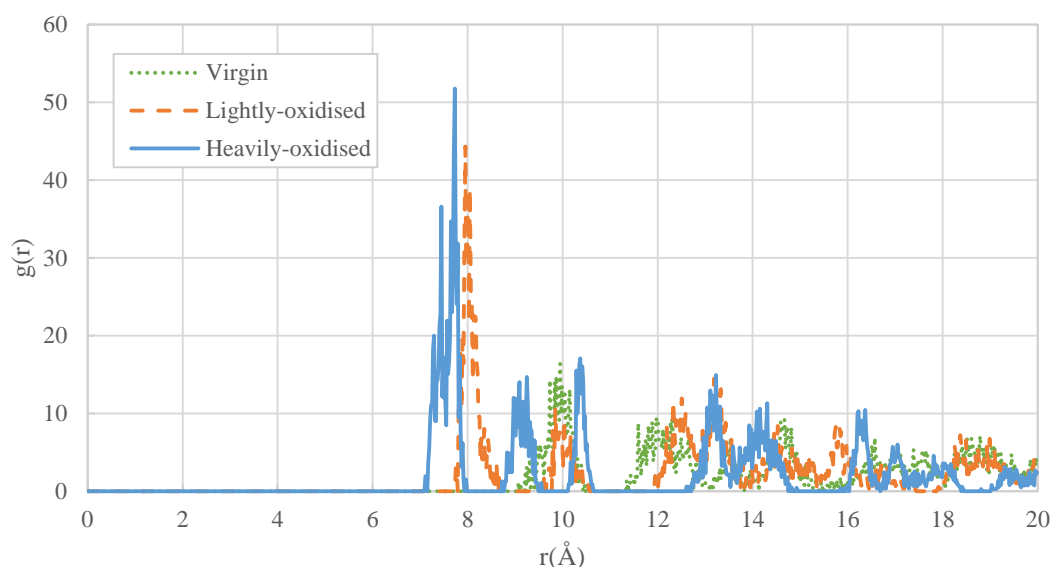


**Fig. 11.** RDFs of asphaltene-asphaltene pair in bitumen-microcline interfacial model at different oxidation levels.

**Table 3** First peak positions of RDF curves for asphaltene-asphaltene pair in bulk bitumen model and four interfacial models at different oxidation levels.

Models	Virgin	Lightly-oxidised	Heavily-oxidised
--------	--------	------------------	------------------

Bulk Bitumen Model	10-11 Å	4-5 Å	8-9 Å
Bitumen-Quartz Model	9-10 Å	6-7 Å	10 Å
Bitumen-Calcite Model	9-10 Å	9 Å	11-12 Å
Bitumen-Albite Model	10-11 Å	11-12 Å	8 Å
Bitumen-Microcline Model	10 Å	8 Å	7-8 Å

MSD is used to study the molecular mobility of bitumen on the mineral surfaces over time that is associated with the interaction between bitumen and minerals. In this study, MSD of bitumen was measured based on the asphaltene molecule's centre of mass. A higher slope of MSD curves means a greater mobility of molecules. **Fig. 12** illustrates the MSDs of asphaltenes in bitumen-microcline interfacial model at different oxidation levels. **Table 4** shows the slopes of MSD curves for asphaltenes in bulk bitumen model and four interfacial models at different oxidation levels. It can be seen that in all these models except for the bitumen-calcite model, the mobility of the oxidised bitumen was smaller than that of the virgin bitumen, which means that the oxidative aging slowed down the mobility of the bitumen molecules. This is because the oxidised bitumen had an enhanced aggregation due to oxidation as well as a larger molecular weight with the introduction of the oxygen atoms. It is noted that the lightly-oxidised bitumen on the calcite surface had a greater molecular mobility since calcite caused the weak aggregation of the lightly-oxidised bitumen that has been shown in **Table 3**. It was also found from **Table 4** that the bitumen molecules on different mineral surfaces exhibits distinctive molecular mobility. The mobility of the bitumen on the quartz and calcite surfaces was faster than that on the albite and microcline surfaces as the strong attraction between bitumen and alkaline minerals (albite and microcline) constrained the mobility of the bitumen molecules.

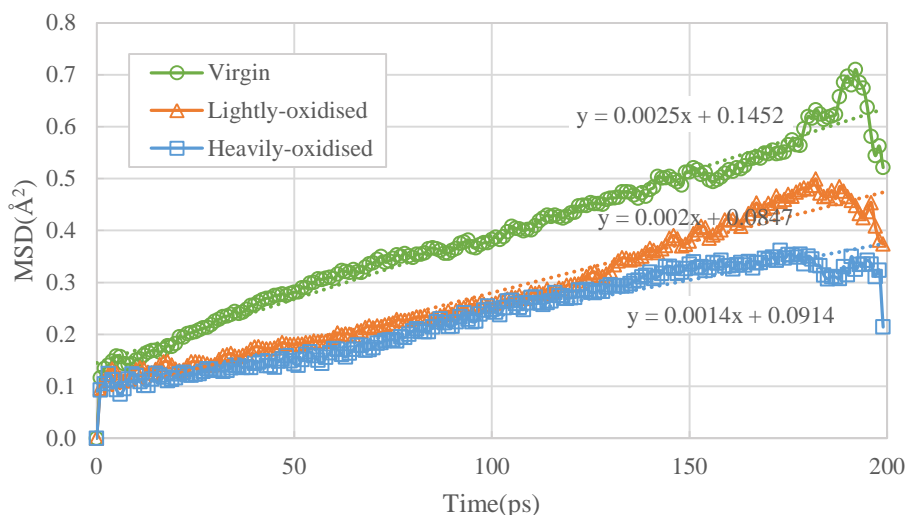


**Fig. 12.** MSDs of asphaltenes in bitumen-microcline interfacial model at different oxidation levels.

**Table 4** Slopes of MSD curves for asphaltenes in bulk bitumen model and four interfacial models at different oxidation levels.

Models	Virgin	Lightly-oxidised	Heavily-oxidised
Bulk Bitumen Model	0.0052	0.0013	0.0050
Bitumen-Quartz Model	0.0124	0.0014	0.0092
Bitumen-Calcite Model	0.0049	0.0139	0.0057
Bitumen-Albite Model	0.0034	0.0031	0.0006
Bitumen-Microcline Model	0.0025	0.0020	0.0014

### 5.3 Effect of oxidative aging on work of adhesion at dry condition

To quantify the adhesion between the bitumen (at different oxidation levels) and the different minerals at the dry condition, the work of adhesion of the bitumen-mineral interface systems was calculated based on the MD simulation results. **Figs. 13** and **15-17** illustrate the work of adhesion for the bitumen-quartz, bitumen-calcite, bitumen-albite and bitumen-microcline interface models at the dry condition and at different oxidative aging levels of the bitumen. It's noted that, based on **Eqs. (1)** and **(2)**, the total energy of a molecular system equals the

summation of valence energy and non-bonded energy, where the non-bonded energy is composed of van der Waals and electrostatic interaction energy. It was found that total energy equalled to the non-bond energy for all of the four bitumen-mineral interface systems, which indicates that the interfacial adhesion between bitumen and mineral purely results from the non-bond interaction and the valence energy does not contribute to the total energy of the bitumen-mineral system. This is consistent with the previous finding that the bitumen-mineral adhesion is attributed to non-bond interaction energy [34].

The work of adhesion of the bitumen-quartz model at the dry condition and at different oxidation levels of the bitumen is shown in **Fig. 13**. It was found that the work of adhesion ( $W_{\text{BM-dry}}$ ) decreased with the increase of the oxidation level, which indicates that the bitumen aging weakens the interfacial adhesion between the bitumen and the quartz. This is in agreement with the experimental finding from Yi et al. [13] who found that the aging of bitumen weakened the bonding performance between bitumen and granite (in which quartz is the major component). The negative effect of aging is due to the decreased van der Waals energy after aging, where the van der Waals is the primary component of the adhesion between the bitumen and the quartz as the electrostatic energy contributes little to the total energy, as indicated in **Fig.13**.

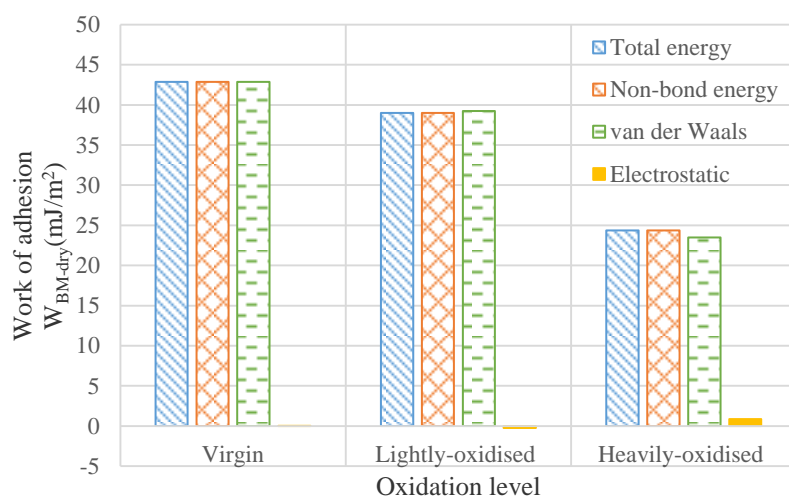


**Fig. 13.** Work of adhesion for bitumen-quartz interface model at the dry condition and different oxidation levels. (Note, based on **Eqs. (1)** and **(2)**, total energy = valence energy + non-bonded energy, and non-bonded energy = van der Waals + electrostatic energy.)

The decreased van der Waals energy is fundamentally caused by the increased distance between the bitumen and quartz molecules when the bitumen becomes aged. In **Fig. 14(a)**, the centre-to-centre distance between the bitumen mass and the quartz matrix was computed. It was found that the centre-to-centre distance of the bitumen-quartz models increased from 30.65 Å ( $10^{-10}$  m) for the virgin bitumen to 31.15 Å and 34.34 Å for the lightly-oxidised bitumen and the heavily-oxidised bitumen, respectively. According to **Eq. (4)**, a greater distance between atoms leads to a lower van der Waals energy. Thus the van der Waals energy between bitumen and quartz is reduced when the bitumen becomes more severely aged. Furthermore, the increased centre-to-centre distance between bitumen and quartz at a higher oxidation level is believed due to the stronger aggregation of the oxidised bitumen molecules, resulting from higher polarity and molecular weight when the oxygen atoms are introduced into the bitumen. In sum, the severer agglomeration of the oxidised bitumen caused by more polar carbonyl and sulfoxide functional groups leads to a greater distance between the mass centre of the bitumen and quartz, which decreases the van der Waals interaction and eventually weakens the work of adhesion of the bitumen-quartz model at the dry condition.

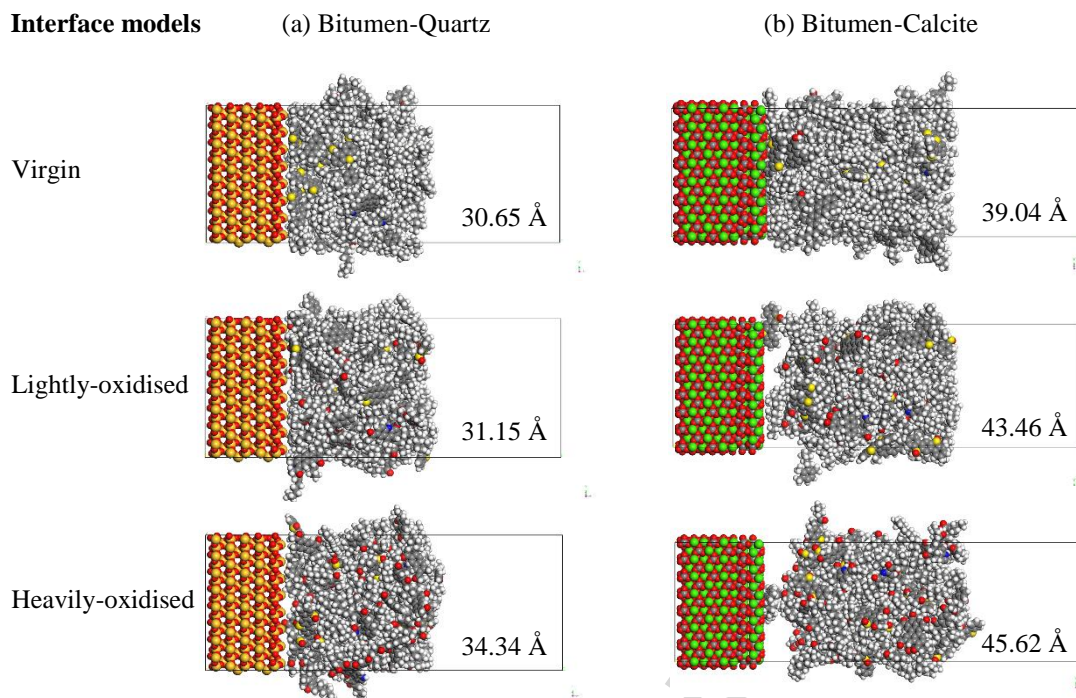


**Fig. 14.** Centre-to-centre distance (Å or  $10^{-10}$  m) between bitumen mass and mineral matrix for (a) bitumen-quartz interface model and (b) bitumen-calcite interface model at different oxidation levels.

**Fig. 15** shows the work of adhesion of the bitumen-calcite interface model at the dry condition and at different oxidation levels. The work of adhesion ( $W_{\text{BM-dry}}$ ) first decreased from  $57.13 \text{ mJ/m}^2$  for the virgin interface model to  $34.97 \text{ mJ/m}^2$  for the lightly-oxidised interface model but then increased to  $61.08 \text{ mJ/m}^2$  for the heavily-oxidised interface model. This change results from the combined aging-induced changes of the van der Waals energy and the electrostatic energy that both contribute to the adhesion between the bitumen and the calcite, as shown in **Fig. 15**. Cucalon et al. [55] also found that, compared to the virgin bitumen, the long-term aged bitumen using a Pressure Aging Vessel test (PAV) has a higher adhesive bond energy with limestone (in which calcite is the main component). The results in **Figure 12** verifies the findings of Cucalon et al [55] from the molecular modelling perspective.

The van der Waals energy is inversely proportional to the distance between atoms according to **Eq. (4)**. It can be seen from **Fig. 14(b)** that the centre-to-centre distance between the

bitumen mass and calcite matrix has increased from 39.04 Å for the virgin bitumen-calcite model to 43.46 Å for the lightly-oxidised bitumen-calcite model and 45.62 Å for the heavily-oxidised bitumen-calcite model, respectively. This leads to a constant decrease of the van der Waals energy with the increasing oxidation level in the bitumen-calcite interface system, which is consistent with the findings for the bitumen-quartz interface system as shown in **Fig. 13**.

However, the electrostatic energy is inversely proportional to the distance between the atoms and directly proportional to the atomic charges according to **Eq. (3)**. When the bitumen becomes more severely aged, the greater bitumen-calcite distance (due to more aggregation of bitumen molecules) causes a lower electrostatic energy and the higher atomic charges (due to more oxygen atoms and higher polarity) results in a higher electrostatic energy. **Fig. 15** shows that the electrostatic energy of the bitumen-calcite interface system decreased when the bitumen became lightly-oxidised and then increased when the bitumen was heavily-oxidised. Thus it may be concluded that the centre-to-centre distance is the dominating factor for determining the electrostatic energy of the lightly-oxidised bitumen-calcite interface system, whereas the atomic charge is the dominating factor for determining the electrostatic energy of the heavily-oxidised bitumen-calcite interface system.

**Fig. 15** also indicates that the electrostatic energy is the primary contributor and the van der Waals energy is the secondary contributor for the non-bonded energy (that is the same as the total energy). Thus the change of the work of adhesion for the bitumen-calcite model is dominantly determined by and follows the same trend as the electrostatic energy, which decreases when bitumen is lightly-oxidised and then increases when the bitumen becomes heavily-oxidised.

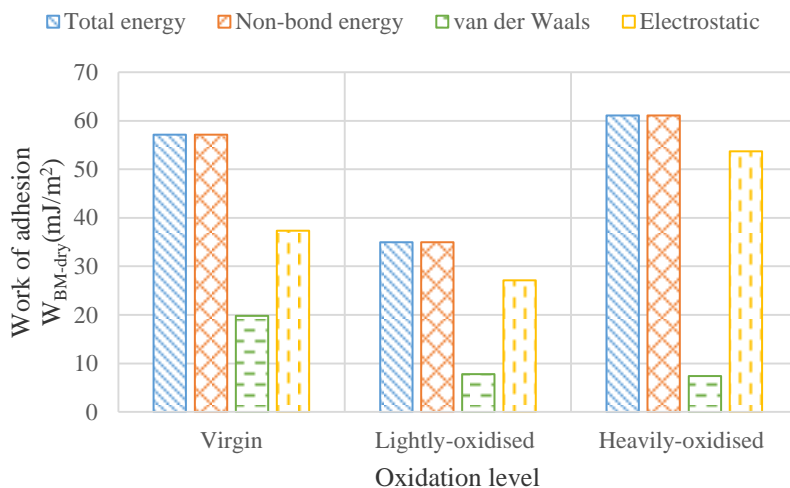


**Fig. 15.** Work of adhesion for bitumen-calcite interface model at dry condition and different oxidation levels. (Note, based on Eqs. (1) and (2), total energy = valence energy + non-bonded energy, and non-bonded energy = van der Waals + electrostatic energy.)

The work of adhesion values of the bitumen-albite model and the bitumen-microcline model at the dry condition and at different oxidation levels are shown in Figs. 16 and 17, respectively. It was found that the work of adhesion ( $W_{BM-dry}$ ) significantly increased with the increase of the oxidation level, which indicates that the oxidation of bitumen is able to strengthen the adhesion for the bitumen-albite interface and the bitumen-microcline interface. This is because of the considerable increase of the electrostatic energy that contributes to the primary interfacial adhesion in the bitumen-albite model and the bitumen-microcline model, as shown in Figs. 16 and 17. The strong electrostatic interaction for the oxidised bitumen-albite or bitumen-microcline interface system is caused by the very strong electrostatic attraction between the negatively charged oxidised bitumen due to the introduction of oxygen atoms during aging and the positively charged alkaline minerals (albite and microcline). It is noted that the van der Waals energy is a very minor contributor to the total energy as shown in Figs. 16 and 17. Thus the work of adhesion is primarily dominated by the electrostatic energy for the bitumen-albite or bitumen-microcline interface system.

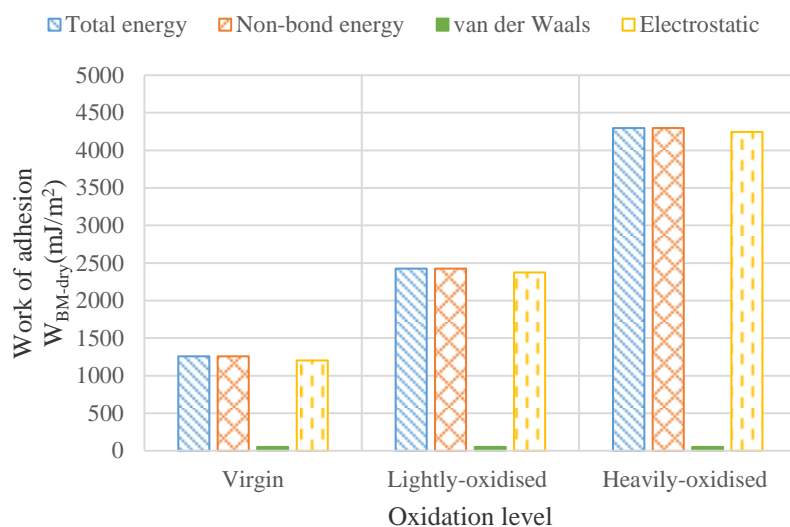


**Fig. 16.** Work of adhesion for bitumen-albite interface model at the dry condition and different oxidation levels. (Note, based on Eqs. (1) and (2), total energy = valence energy + non-bonded energy, and non-bonded energy = van der Waals + electrostatic energy.)

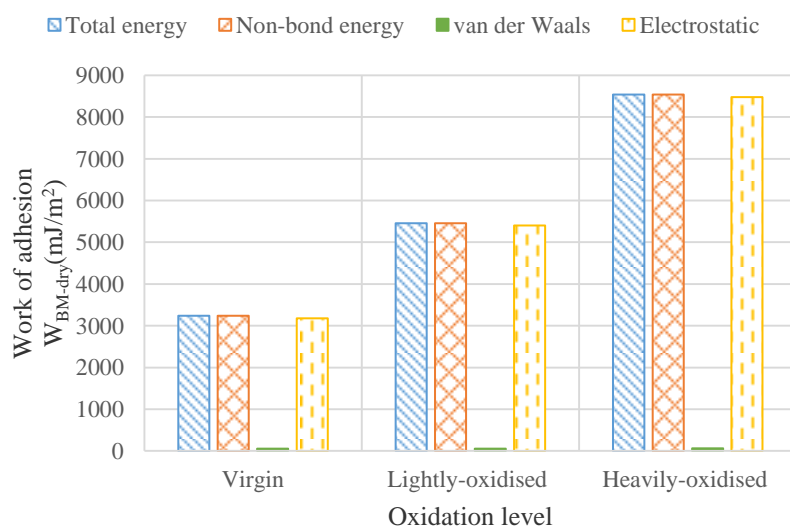


**Fig. 17.** Work of adhesion for bitumen-microcline interface model at the dry condition and different oxidation levels. (Note, based on Eqs. (1) and (2), total energy = valence energy + non-bonded energy, and non-bonded energy = van der Waals + electrostatic energy.)

As observed above, the variation of the work of adhesion for the four bitumen-mineral models at dry condition is significantly distinct when bitumen becomes more severely aged (decrease for the bitumen-quartz model, decrease and then increase for the bitumen-calcite model, and

increase for the bitumen-albite model and the bitumen-microcline model). The difference results from the different chemical properties of the minerals. Quartz is an acidic mineral, having a rather weak or negligible electrostatic interaction with the acidic bitumen, while albite and microcline are the strongly alkaline minerals, having a considerably strong electrostatic interaction with the oxidised bitumen containing more polar molecules. Calcite presents weakly alkaline, having a relatively weak electrostatic interaction with the acidic bitumen. The previous experimental studies [56] and molecular simulation results [34] have shown that a mineral with an alkaline nature has a stronger electrostatic adhesion with the weakly acidic bitumen than an acidic mineral. Therefore, it can be concluded that the effect of bitumen oxidative aging on the bitumen-mineral interfacial adhesion strongly depends on the mineral types.

#### *5.4 Effect of oxidative aging on work of adhesion at wet condition*

To study the effect of water on the oxidised bitumen-mineral adhesion, the work of adhesion of the four bitumen-mineral interface systems at wet condition and different oxidation levels was also calculated based on the MD simulation results and was compared with the work of adhesion at dry condition, as shown in **Figs. 18-21**.

The work of adhesion of the bitumen-quartz model at dry and wet conditions with different oxidation levels is shown in **Fig. 18**. It can be seen that the work of adhesion at wet condition had little change with the oxidation level, which indicates that the oxidative aging has a very weak or none influence on the bitumen-quartz interfacial adhesion at the wet condition. This is because the already very low van der Waals interaction (serving as the major contributor to the bitumen-quartz adhesion) at wet condition cannot be further reduced by the stronger aggregation of the oxidised bitumen at the aging condition. **Fig. 18** also shows that the work of adhesion was much smaller at the wet condition as compared to that at the dry condition.

This is because the presence of water molecules has separated the bitumen from the quartz and increased the distance between the bitumen molecules and the quartz atoms, leading to the very weak van der Waals interaction according to **Eq. (4)**.

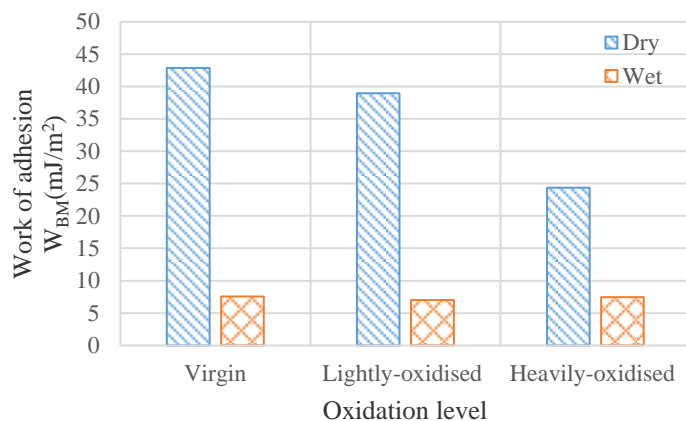


**Fig. 18.** Work of adhesion of bitumen-quartz model at dry and wet conditions and different oxidation levels.

**Fig. 19** shows the work of adhesion of the bitumen-calcite model at dry and wet conditions with different oxidation levels. It was found that the work of adhesion for the oxidised bitumen-calcite model was slightly greater than that of the virgin model at the wet condition, which indicates that the oxidation of bitumen has made the bitumen-calcite adhesion stronger at the wet condition. This is because of the increase of the electrostatic interaction between bitumen and calcite. This explains the findings from Cucalon et al. [55] that the resistance of the interfacial bonding between bitumen and limestone to moisture damage improves when the bitumen becomes aged. **Fig. 19** also shows that the work of adhesion at wet condition was always smaller than that at dry condition since the presence of water molecules makes the bitumen-calcite van der Waals interaction weaker. This means that water tends to weaken the adhesion between bitumen and calcite, which remains consistent with the bitumen-quartz model.

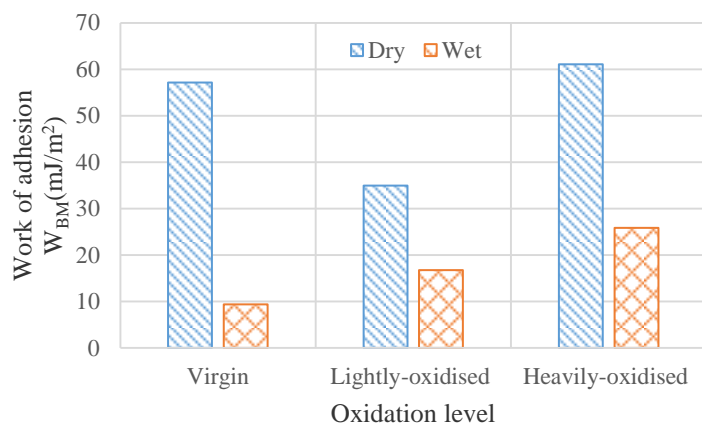


**Fig. 19.** Work of adhesion of the bitumen-calcite model at dry and wet conditions and different oxidation levels.

The work of adhesion values of the bitumen-albite model and the bitumen-microcline model at dry and wet conditions and different oxidation levels are shown in **Figs. 20** and **21**, respectively. It was found that the work of adhesion at both dry and wet conditions significantly increased with the increase of oxidation level, which indicates that the oxidative aging has been able to strengthen the interfacial adhesion for the bitumen-albite model and the bitumen-microcline model, regardless the effect of water. This results from the considerable increase of the electrostatic interaction which is the major contributor to the interfacial adhesion of the bitumen-albite model and the bitumen-microcline model. From **Fig. 20** and **21**, it can be seen that the work of adhesion at wet condition was very close to and consistent with that at dry condition. This differs from the case of the bitumen-quartz model and the bitumen-calcite model where the work of adhesion at wet condition was always weaker than that at the dry condition, as shown in **Figs. 18** and **19**. This difference is mainly caused by the much stronger electrostatic interaction at the bitumen-albite interface and the bitumen-microcline interface, resulting from the stronger attraction between the highly alkaline minerals (albite and microcline) and the oxidised bitumen with the high polarity due to oxidative aging.

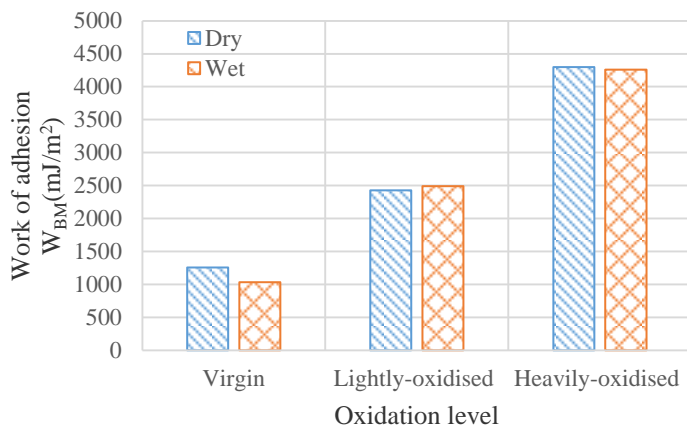


**Fig. 20.** Work of adhesion of the bitumen-albite model at dry and wet conditions and different oxidation levels.

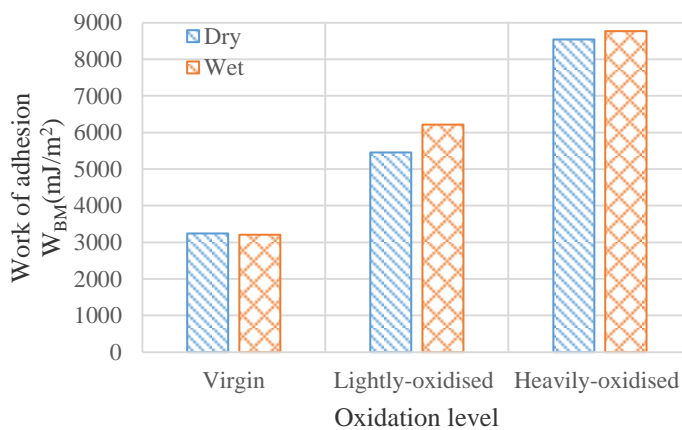


**Fig. 21.** Work of adhesion of the bitumen-microcline model at dry and wet conditions and different oxidation levels.

### 5.5 Combined effect of oxidative aging and water on bitumen-mineral interfacial adhesion

To clearly describe the combined effects of oxidative aging and water on the bitumen-mineral adhesion at wet condition, the sensitivity of adhesion to oxidative aging ( $S_O$ ) and the sensitivity of adhesion to water ( $S_W$ ) are proposed using the work of adhesion. The sensitivity of adhesion to oxidative aging ( $S_O$ ) at wet condition is defined as the difference of the work of adhesion before and after oxidative aging divided by the work of adhesion before oxidative aging, as shown in **Eq. (7)**. The sensitivity of adhesion to water ( $S_W$ ) is calculated as the ratio of the change of the work of adhesion from dry to wet conditions as compared to the work of

adhesion at dry condition, as expressed in Eq. (8). A higher absolute value of the sensitivity of adhesion ( $S_O$  or  $S_W$ ) means a greater effect of oxidative aging or water on the bitumen-mineral adhesion. A positive (or negative) value of the sensitivity of adhesion ( $S$ ) indicates the strengthening (or weakening) effect.

$$S_{O-H} = (W_{BM-H} - W_{BM-V}) / W_{BM-V} \quad \text{or} \quad S_{O-L} = (W_{BM-L} - W_{BM-V}) / W_{BM-V} \quad (7)$$

$$S_W = (W_{BM-wet} - W_{BM-dry}) / W_{BM-dry} \quad (8)$$

where  $W_{BM-H}$ ,  $W_{BM-L}$ , and  $W_{BM-V}$  are the work of adhesion between bitumen and mineral at wet condition for heavily-oxidised, lightly-oxidised and virgin bitumens, respectively; and  $W_{BM-dry}$  and  $W_{BM-wet}$  are the work of adhesion between bitumen and mineral at dry and wet conditions, respectively.

**Fig. 22** shows the sensitivity of adhesion to the oxidative aging ( $S_{O-H}$  and  $S_{O-L}$ ) and water ( $S_W$ ) for quartz (acidic), calcite (weak alkali) and albite (strong alkali) minerals. It can be seen that the sensitivity of the bitumen-mineral adhesion to the oxidative aging becomes higher and the absolute sensitivity of the bitumen-mineral adhesion to water becomes lower when the mineral changes from acidic to weak alkali and to strong alkali types.

This is fundamentally due to that, for the acidic minerals, van der Waals energy is the major contributor for bitumen-mineral adhesion which can be significantly reduced by water through increasing the distance between the bitumen and the acidic minerals. In this case, the electrostatic energy of the acidic mineral with the acidic bitumen is so weak that the increase of the polarity of the bitumen due to aging will not alter the overall adhesion between the bitumen and the acidic minerals. Therefore, the adhesion of the acidic minerals (such as quartz) with bitumen is more susceptible to the water but much less sensitive to the bitumen aging.

For the strong alkali minerals, the electrostatic energy is much higher than the van der Waals

energy and becomes the dominating contributor to the bitumen-mineral adhesion. The electrostatic energy becomes even higher when the bitumen is aged due to higher polarity of the oxidised bitumen. However, the van der Waals is so minor for the adhesion between bitumen and the strong alkali minerals that the decrease of the van der Waals due to water cannot alter the adhesion significantly. Thus the adhesion of the strong alkali minerals (such as albite and microcline) with bitumen is more susceptible to bitumen aging but less sensitive to water.

For the weak alkali minerals, both the van der Waals and the electrostatic energy contribute to the adhesion with bitumen. The van der Waals energy can be significantly reduced by water due to greater distance and the electrostatic energy can be dramatically increased by bitumen aging due to higher polarity. Thus the adhesion of the weak alkali mineral (such as calcite) with bitumen is susceptible to both bitumen aging and the water.



**Fig. 22.** Sensitivity of adhesion to oxidative aging ( $S_{O-H}$  and  $S_{O-L}$ ) and water ( $S_W$ ) for quartz (acidic), calcite (weak alkali) and albite (strong alkali) minerals.

## 6. Summary and conclusions

A study has been conducted to discover the interfacial adhesion mechanism between oxidised

bitumen and mineral surfaces at dry and wet conditions using molecular dynamics simulation method. Based on the results, the main conclusions are as follows:

(1) The oxidised functional groups (i.e., carbonyl and sulfoxide) in bitumen due to oxidative aging strengthens the intermolecular bonding of the bitumen including van der Waals and electrostatic interactions, which results in the aggregation of bitumen molecules and physical hardening of the aged bitumen. This is revealed by the increase of density and cohesive energy density and the decrease of the fraction of free volume, when the bitumen becomes oxidative aging.

(2) When bitumen becomes more severely aged at dry condition, the adhesive bond energy consistently decreases for bitumen-quartz (an acidic mineral) interface, decreases first and then increases for the bitumen-calcite (a weak alkali mineral) interface, and constantly increases for the bitumen-albite or microcline (strong alkali minerals) interfaces.

(3) The interfacial adhesion of bitumen-acidic minerals (e.g., quartz) at dry condition is dominated by van der Waals interaction which decreases when bitumen becomes aged. This is due to the increased bitumen-quartz distance caused by the aggregated bitumen molecules. In comparison, the interfacial adhesion of bitumen-strong alkali minerals (e.g., albite and microcline) is dominated by electrostatic energy which increases during aging. This results from the higher polarity introduced by the oxidised products including carbonyl and sulfoxide in an aged bitumen.

(4) The interfacial adhesion of bitumen-weak alkali mineral (calcite) at dry condition is attributed primarily to electrostatic energy and secondarily to van der Waals energy. The electrostatic energy between aged bitumen and the weak alkali mineral decreases due to the increased bitumen-mineral distance when the bitumen is lightly-oxidised and increases due to the higher bitumen polarity when the bitumen is heavily-oxidised.

(5) For the bitumen-mineral interfacial adhesion at wet condition, water is the dominating factor that affects (weakens) the interfacial adhesion between the bitumen and the acidic minerals such as quartz. While the oxidative aging of bitumen is the major factor that affects (strengthens) the interfacial adhesion between the bitumen and the strongly alkaline minerals (i.e., albite and microcline). For the weak alkali minerals such as calcite, both water and bitumen aging can significantly affect the interfacial adhesion.

The research findings provide a fundamental understanding of the interfacial adhesion between oxidised bitumen and mineral surfaces at dry and wet conditions from the perspective of molecular modelling. The results can potentially be used for guiding the paring and selections of the virgin and aged bitumen (such as reclaimed asphalt binder) with different minerals for optimal performance of asphalt mixtures. Further work will be focused on studying the effect of bitumens aging on the cohesive and interfacial adhesive debonding under various loading conditions for the asphalt materials.

### **Acknowledgements**

The authors acknowledge the financial support provided by Aston University via a PhD studentship and by European Union's Horizon 2020 programme via a Marie S. Curie Individual Fellowship project (Grant No. 749232 - AMAM).

### **References**

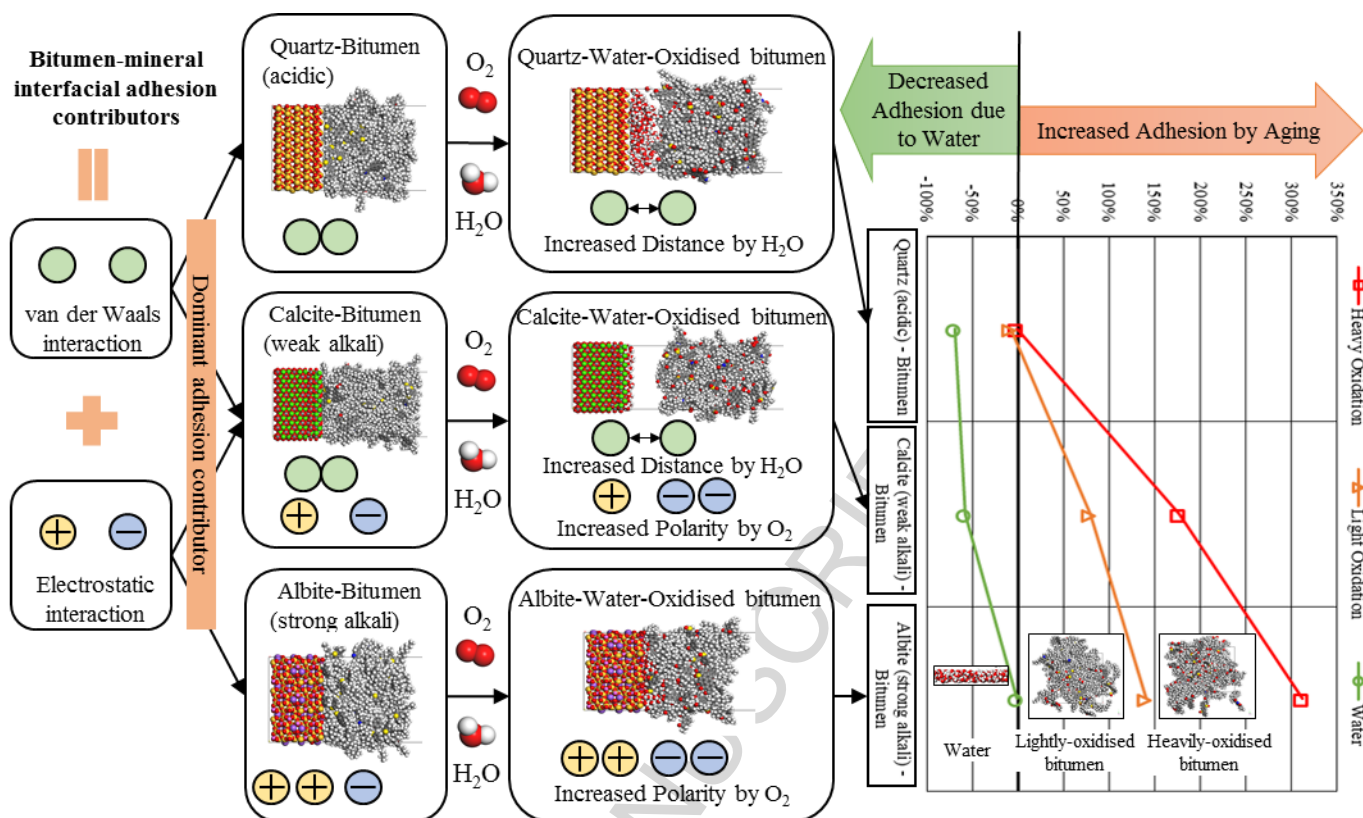
- [1] Gu F, Ma W, West R C, Taylor AJ, Zhang Y. Structural performance and sustainability assessment of cold central-plant and in-place recycled asphalt pavements: A case study. *J Clean Prod* 2019;208:1513-23.
- [2] Wu SP, Liu XM, Ye QS, LI N. Self-monitoring electrically conductive asphalt-based composite containing carbon fillers. *Trans Nonferrous Met Soc China* 2006;16:512-6.
- [3] Petersen JC. Chemical composition of asphalt as related to asphalt durability: state of the art. *Transport Res Rec* 1984;999:13-30.
- [4] Knorr DB, Davison RR, Glover CJ. Effect of various aging techniques on asphalt low-temperature

- properties. *Transport Res Rec* 2002;1810:9-16.
- [5] Das PK, Balieu R, Kringos N, Birgisson B. On the oxidative ageing mechanism and its effect on asphalt mixtures morphology. *Mater Struct* 2015;48:3113-27.
- [6] Andersen SI, Birdi KS. Aggregation of asphaltenes as determined by calorimetry. *J Colloid Interf Sci* 1991;142:497-502.
- [7] Jennings PW, Pribanic JA, Fanconi B, VanderHart DL. Binder characterization and evaluation by nuclear magnetic resonance spectroscopy. Report SHRP-A-335; Strategic Highway Research Program, National Research Council: Washington, D.C., 1993.
- [8] Collop AC, Choi Y, Airey GD. Effects of pressure and aging in SATS test. *J Transp Eng-ASCE* 2007;133(11):618-24.
- [9] National Cooperative Highway Research Program (NCHRP). Simulating the effects of hot mix asphalt aging for performance testing and pavement structural design. National Cooperative and Highway Research Report; Transportation Research Board: Washington, D.C., 2007; Research Results Digest 324.
- [10] Qin Q, Schabronb JF, Boysenb RB, Farrarb MJ. Field aging effect on chemistry and rheology of asphalt binders and rheological predictions for field aging. *Fuel* 2014;121:86-94.
- [11] Yang Y, Zhang Y, Omairey E, Cai J, Gu F, Bridgwater AV. Intermediate pyrolysis of organic fraction of municipal solid waste and rheological study of the pyrolysis oil for potential use as bio-bitumen. *J Clean Prod* 2018;187:390-9.
- [12] Bhasin A, Palvadi S, Little DN. Influence of aging and temperature on intrinsic healing of asphalt binders. *Transport Res Rec* 2011;2207:70-8.
- [13] Yi JY, Pang XY, Feng DC, Pei ZS, Xu M, Xie SN, Huang YD. Studies on surface energy of asphalt and aggregate at different scales and bonding property of asphalt-aggregate system. *Road Mater Pavement* 2017; DOI:10.1080/14680629.2017.1300597
- [14] Petersen JC. A review of the fundamentals of asphalt oxidation: chemical, physicochemical, physical property, and durability relationships. Transportation Research E-Circular E-C140. Washington (DC): Transportation Research Board; 2009.
- [15] Petersen JC, Harnsberger PM. Asphalt aging: dual oxidation mechanism and its interrelationships with asphalt composition and oxidative age hardening. *Transport Res Rec* 1998;1638:47-55.
- [16] Guern ML, Chailleux E, Farcas F, Dreessen S, Mabilie I. Physico-chemical analysis of five hard bitumens: identification of chemical species and molecular organization before and after artificial aging. *Fuel* 2010;89(11):3330-9.

- [17] Hou Y, Wang L, Wang D, Liu P, Guo M, Yu J. Characterization of Bitumen Micro-mechanical Behaviors Using AFM, Phase Dynamics Theory and MD Simulation. *Materials* 2017;10,208; doi:10.3390/ma10020208
- [18] Tarefder RA, Arisa I. Molecular dynamic simulations for determining change in thermodynamic properties of asphaltene and resin because of aging. *Energy Fuels* 2011;25:2211-22.
- [19] Groenzing HG; Mullins OC. Molecular size and structure of asphaltenes from various sources. *Energy Fuels* 2000;14:677-84.
- [20] Murgich J, Rodriguez J, Aray Y. Molecular recognition and molecular mechanics of micelles of some model asphaltenes and resins. *Energy Fuels* 1996;10:68-76.
- [21] Pan T, Lu Y, Lloyd S. Quantum-chemistry study of asphalt oxidative aging: an XPS-aided analysis. *Ind Eng Chem Res* 2012;51:7957-66.
- [22] Zhang L, Greenfield ML. Analyzing properties of model asphalts using molecular simulation. *Energy Fuels* 2007;21:1712-16.
- [23] Li DD, Greenfield ML. Chemical compositions of improved model asphalt systems for molecular simulations. *Fuel* 2014;115:347-56.
- [24] Li DD, Greenfield ML. Viscosity, relaxation time, and dynamics within a model asphalt of larger molecules. *J Chem Phys* 2014;140:1-11.
- [25] Pan JL, Tarefder RA. Investigation of asphalt aging behavior due to the oxidation using molecular dynamics simulation. *Mol Simulat* 2016;42(8):667-78.
- [26] Xu GJ, Wang H. Molecular dynamics study of oxidative aging effect on asphalt binder properties. *Fuel* 2017;188:1-10.
- [27] Gao YM, Dong MS, Li LL, Wang LN, Sun ZB. Interface effects on the creep characteristics of asphalt concrete. *Construction and Building Materials* 2015;96:591-8.
- [28] Dong MS, Gao YM, Li LL, Wang LN, Sun ZB. Viscoelastic micromechanical model for dynamic modulus prediction of asphalt concrete with interface effects. *J Cent South Univ* 2016;23:926-33.
- [29] Lytton RL, Zhang YQ, Gu F, Luo X. Characteristics of damaged asphalt mixtures in tension and compression. *Int J of Pavement Eng* 2018;19(3):292-306.
- [30] Zhang YQ, Luo X, Luo R, Lytton RL. Crack initiation in asphalt mixtures under external compressive loads. *Constr Build Mater* 2014;72:94-103.
- [31] Zhang YQ, Gu F, Birgisson B, Lytton RL. Modelling cracking damage of asphalt mixtures under compressive monotonic and repeated loads using pseudo J-integral Paris' law. *Road Mater Pavement*

- 2018;19(3):525-35.
- [32] Fischer HR, Dillingh EC, Hermse CGM. On the interfacial interaction between bituminous binders and mineral surfaces as present in asphalt mixtures. *Appl. Surf. Sci.* 2013;265:495-9.
- [33] Min YH, Fang Y, Huang XJ, Zhu YH, Li WS, Yuan JM, Tan LG, Wang SY, Wu ZJ. Surface modification of basalt with silane coupling agent on asphalt mixture moisture damage. *Appl. Surf. Sci.* 2015;346:497-502.
- [34] Gao YM, Zhang YQ, Gu F, Xu T, Wang H. Impact of minerals and water on bitumen-mineral adhesion and debonding behaviours using molecular dynamics simulations. *Constr Build Mater* 2018; 171:214-22.
- [35] Amin JS, Nikooee E, Ghatee MH, Ayatollahi S, Alamdari A, Sedghamiz T. Investigating the effect of different asphaltene structures on surface topography and wettability alteration. *Appl. Surf. Sci.* 2011;257:8341-49.
- [36] Li DD, Greenfield ML. High internal energies of proposed asphaltene structures. *Energy Fuels* 2011;25:3698-705.
- [37] Mullins OC. The modified yen model. *Energy Fuels* 2010;24:2179-207.
- [38] Lesueur D. The colloidal structure of bitumen: consequences on the rheology and on the mechanisms of bitumen modification. *Adv Colloid Interface Sci* 2009;145:42-82.
- [39] Oldenburg TBP, Huang H, Donohoe P, Willsch H, Larter SR. High molecular weight aromatic nitrogen and other novel hopanoid-related compounds in crude oils. *Org Geochem* 2004;35:665-78.
- [40] Koopmans MP, De Leeuw JW, Lewan MD, Damsté JSS. Impact of dia- and catagenesis on sulphur and oxygen sequestration of biomarkers as revealed by artificial maturation of an immature sedimentary rock. *Org Geochem* 1996;25:391-426.
- [41] Koopmans MP, De Leeuw JW, Damsté JSS. Novel cyclised and aromatised diagenetic products of  $\beta$ -carotene in the Green River shale. *Org Geochem* 1997;26:451-66.
- [42] Marynowski L, Rospondek MJ, Reckendorf RM, Simoneit BRT. Phenylidibenzofurans and phenylidibenzothiophenes in marine sedimentary rocks and hydrothermal petroleum. *Org Geochem* 2002;33:701-14.
- [43] Cai C, Zhang C, Cai L, Wu G, Jiang L, Xu Z, Li K, Ma A, Chen L. Origins of palaeozoic oils in the Tarim basin: evidence from sulfur isotopes and biomarkers. *Chem Geol* 2009;268:197-210.
- [44] Lira-Galeana C, Hammami A. Wax precipitation from petroleum fluids: a review. In: Yen TF, Chilingarian GV, editors. *Asphalts and asphaltenes, 2. Developments in petroleum science series, vol. 40B*. New York: Elsevier; 2000. p. 557-608.
- [45] Simanzhenkov V, Idem R. *Crude oil chemistry*. New York: Marcel Dekker, Inc.; 2003.

- [46] Netzel DA, Rovani JF. Direct separation and quantitative determination of (n-, iso-) alkanes in neat asphalt using urea adduction and high-temperature gas chromatography (HTGC). *Energy Fuels* 2007;21:333-8.
- [47] Petersen JC, Glaser R. Asphalt oxidation mechanisms and the role of oxidation products on age hardening revisited. *Road Mater Pavement* 2011;12:795-819.
- [48] King WH, Corbett LW. Relative oxygen absorption and volatility properties of submicron films of asphalt using the quartzite crystal microbalance. *Anal Chem* 1969;41:580-83.
- [49] Sun H. COMPASS: an ab initio force-field optimized for condensed-phase applications-overview with details on alkane and benzene compounds. *J Phys Chem B* 1998;102:7338-64.
- [50] Zhang XF, Lu GW, Wen XM, Yang H. Molecular dynamics investigation into the adsorption of oil-water-surfactant mixture on quartz. *Appl. Surf. Sci.* 2009;255:6493-98.
- [51] Dong ZJ, Liu ZY, Wang P, Gong XB. Nanostructure characterization of asphalt-aggregate interface through molecular dynamics simulation and atomic force microscopy, *Fuel* 2017;189:155-163.
- [52] Peng Z, Ewig CS, Hwang MJ, Waldman M, Hagler A T. Derivation of Class II Force Fields, 4. Van der Waals Parameters of Alkali Metal Cations and Halide Anions. *J Phys Chem A* 1997;101:7243-52.
- [53] Jones DR. SHRP materials reference library: asphalt cements: a concise data compilation. Vol. 1. Washington, DC: Strategic Highway Research Program, National Research Council; 1993.
- [54] Wang P, Dong ZJ, Tan YQ, Liu ZY. Investigating the interactions of the saturate, aromatic, resin, and asphaltene four fractions in asphalt binders by molecular simulations. *Energy Fuels* 2015;29:112-21.
- [55] Cucalon LG, Kassem E, Little DN, Masad E. Fundamental evaluation of moisture damage in warm-mix asphalts. *Road Mater Pavement* 2017; 18:sup1, 258-283, DOI: 10.1080/14680629.2016.1266765
- [56] Mirzababaei P. Effect of zycotherm on moisture susceptibility of Warm Mix Asphalt mixtures prepared with different aggregate types and gradations. *Constr Build Mater* 2016;116:403-12.



Graphical abstract

**Highlights**

Paper “Molecular dynamics investigation of interfacial adhesion between oxidised bitumen and mineral surfaces”

- Van der Waals forces dominate interfacial interaction of bitumen with acidic minerals.
- Electrostatic forces dominate interfacial interaction of bitumen with alkali minerals.
- Oxidation causes molecular aggregation and higher polarity of the bitumen.
- Water weakens while oxidation strengthens bitumen-mineral interfacial adhesion.
- Coupled effect of water and oxidation on adhesion depends on mineral’s acid-base.

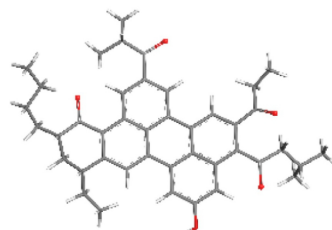
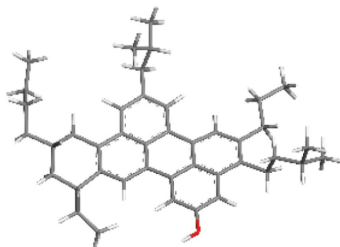
ACCEPTED MANUSCRIPT

# Asphaltenes

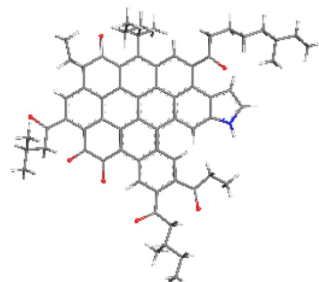
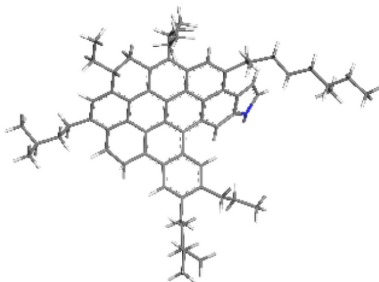
(a) Virgin

(b) Oxidised

AS-1



AS-2



AS-3

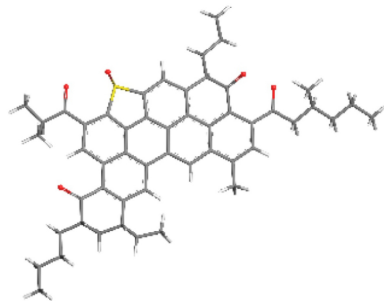
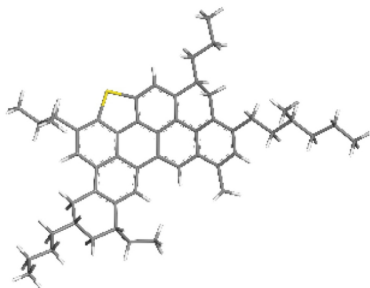


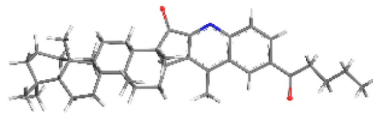
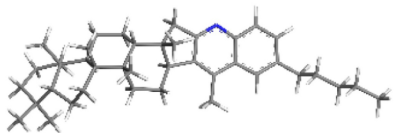
Figure 1

# Resins

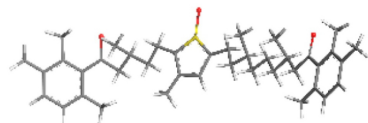
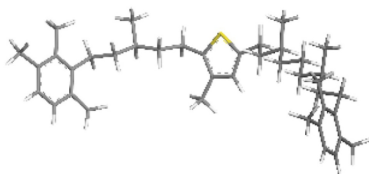
(a) Virgin

(b) Oxidised

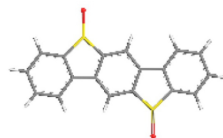
RE-1



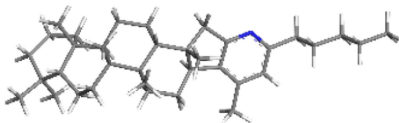
RE-2



RE-3



RE-4



RE-5

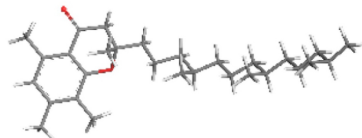


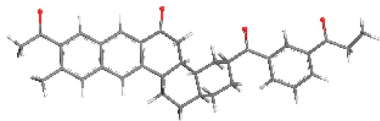
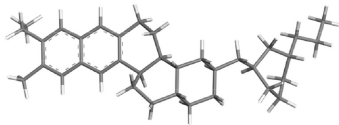
Figure 2

# Aromatics

(a) Virgin

(b) Oxidised

AR-1



AR-2

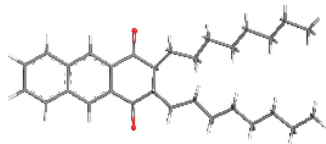
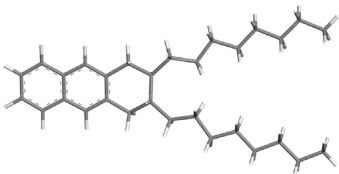
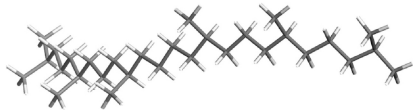
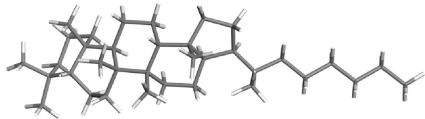


Figure 3

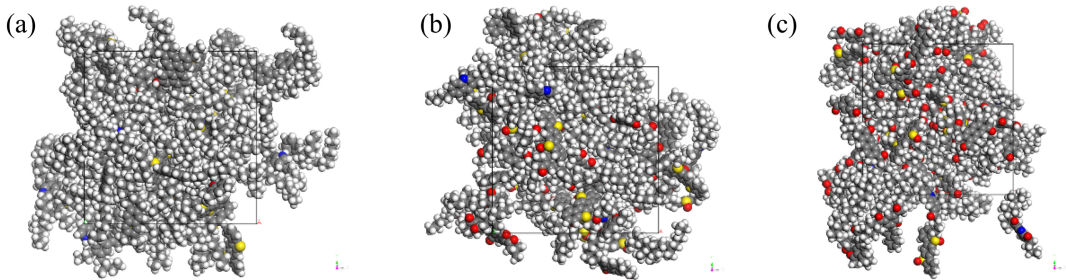


**SA-1**



**SA-2**

Figure 4



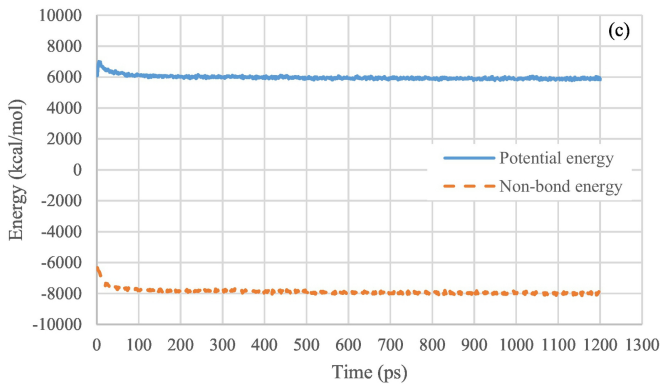
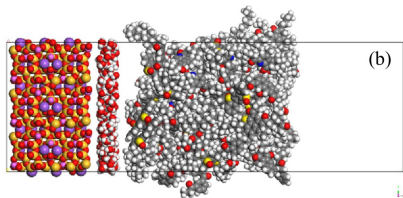
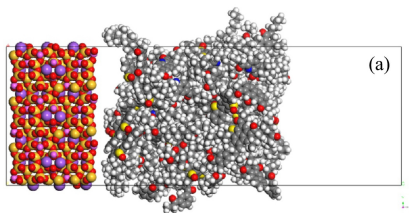


Figure 6

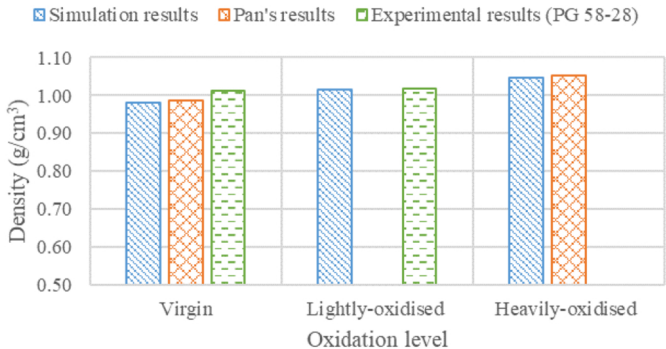


Figure 7

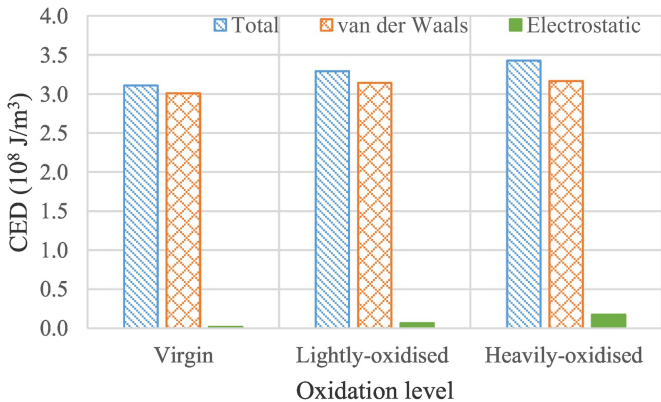


Figure 8

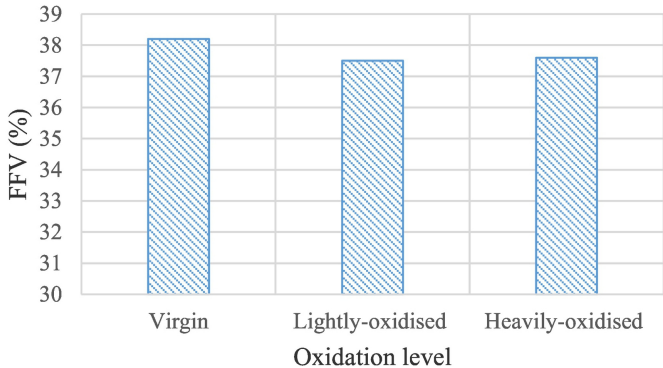
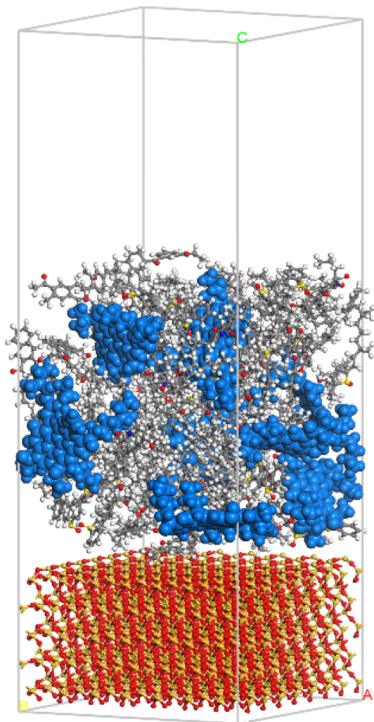
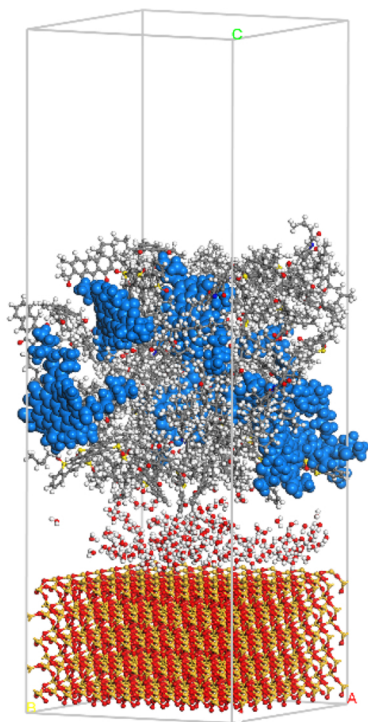


Figure 9



(a)



(b)

Figure 10

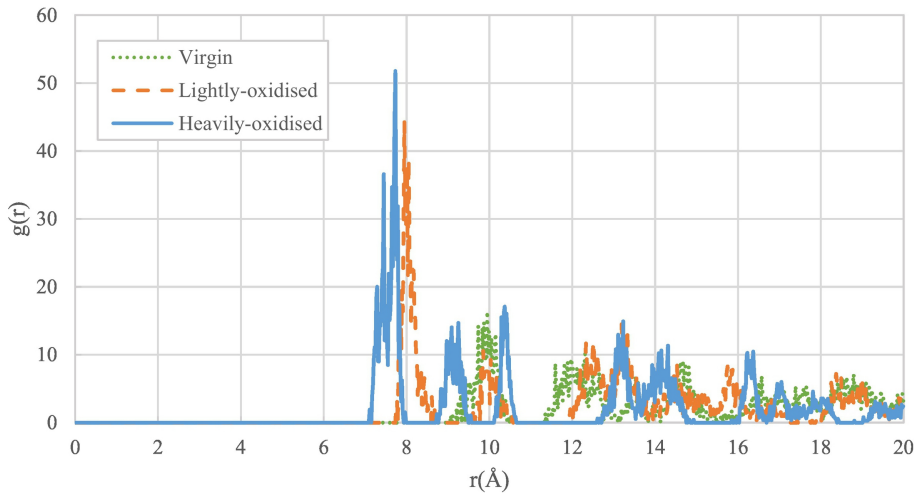


Figure 11

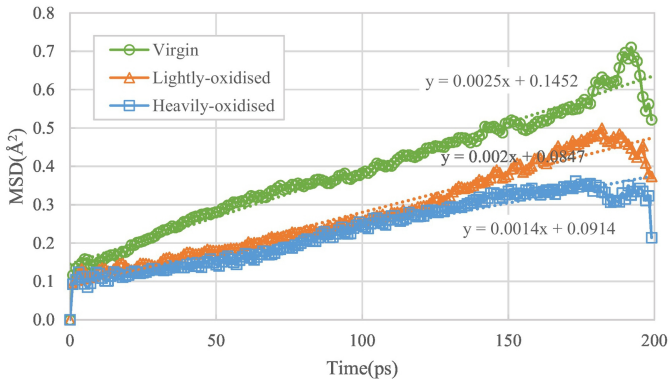


Figure 12

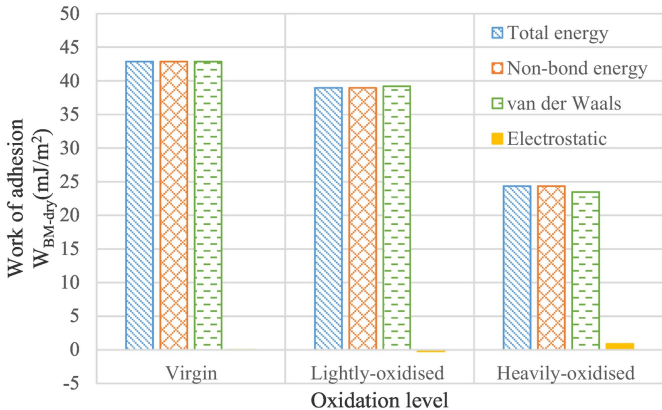


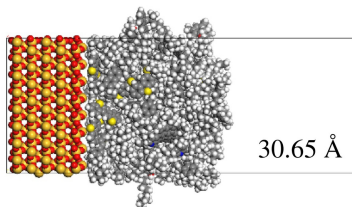
Figure 13

**Interface models**

(a) Bitumen-Quartz

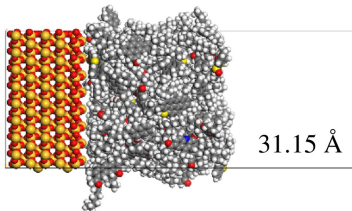
(b) Bitumen-Calcite

Virgin



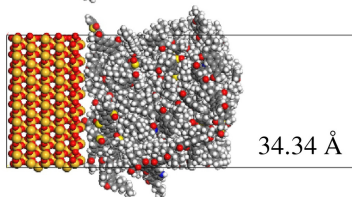
30.65 Å

Lightly-oxidised

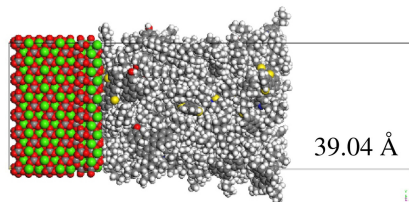


31.15 Å

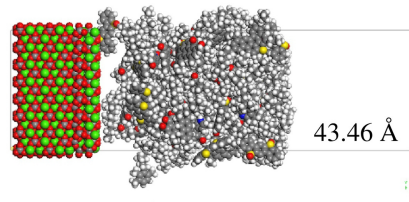
Heavily-oxidised



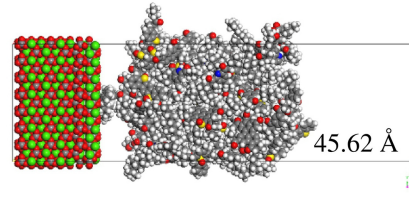
34.34 Å



39.04 Å



43.46 Å



45.62 Å

Figure 14

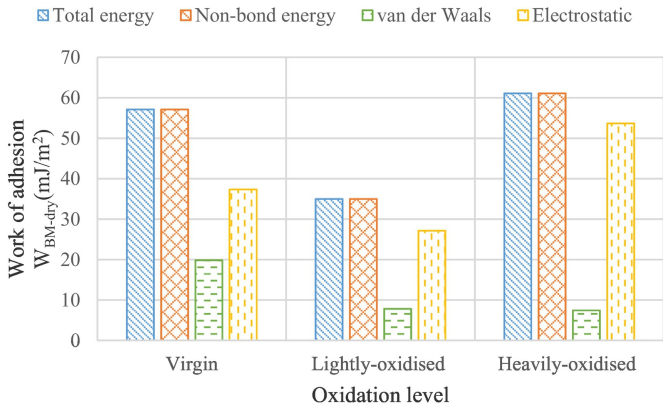


Figure 15

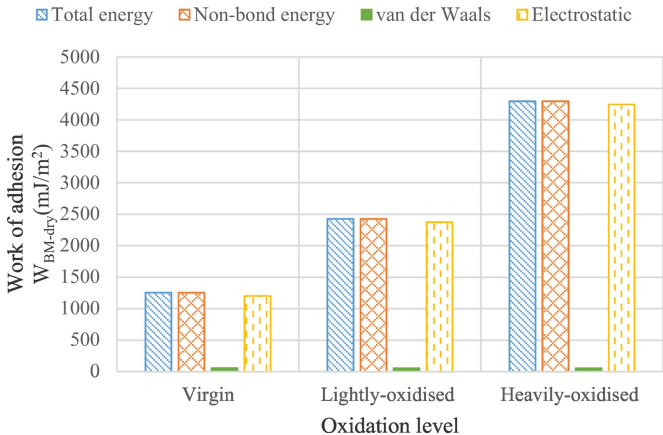


Figure 16

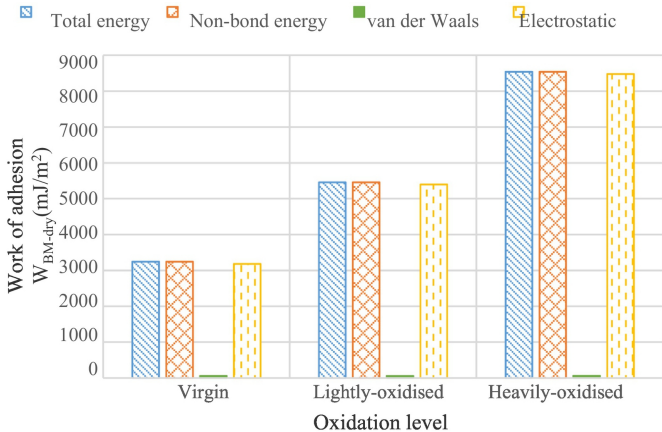


Figure 17

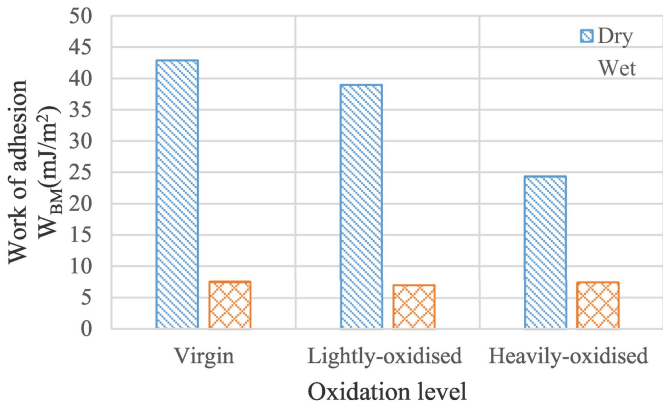


Figure 18

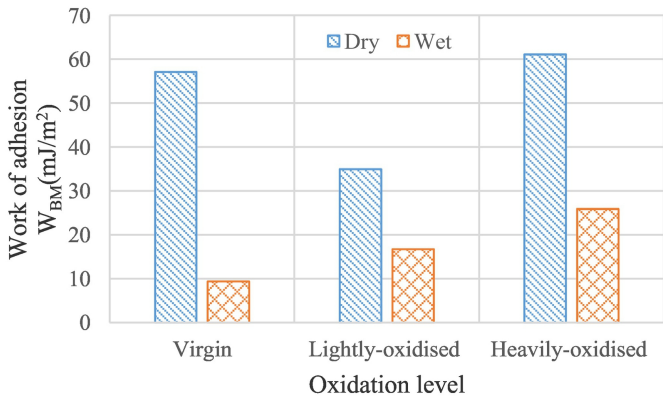


Figure 19

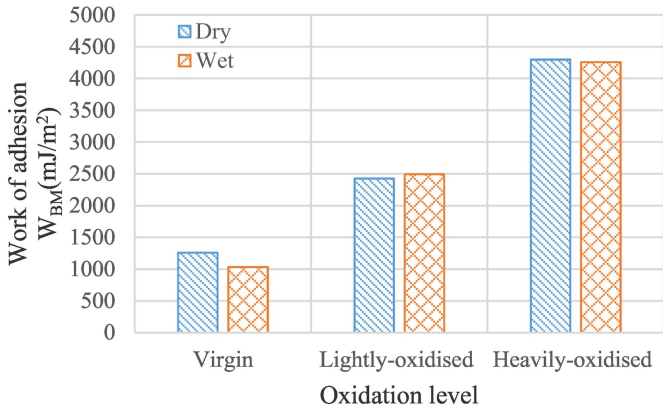


Figure 20

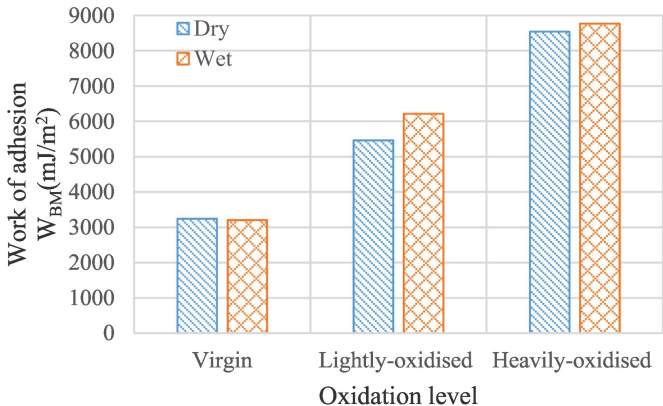


Figure 21

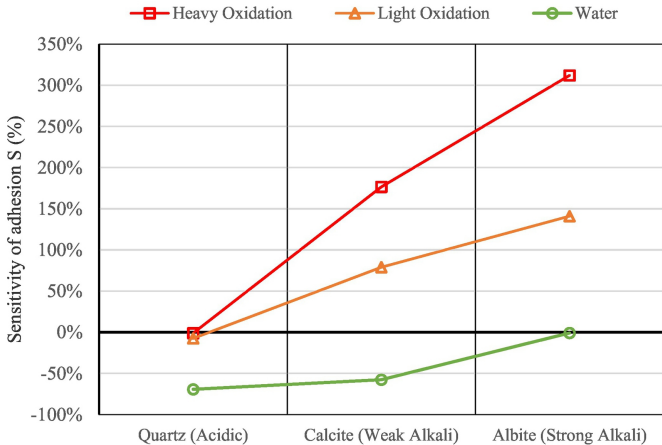


Figure 22